26. Freathy RM, Weedon MN, Shields B, et al. Functional variation in VEGF is not associated with type 2 diabetes in a United Kingdom Caucasian population. *JOP.* 2006;7:295–302.
27. Fernandez-Robredo P, Maestre SR, Zarranz-Ventura J, Mulero HH, Salinas-Alaman A, Garcia-Layana A. Myopic choroidal neovascularization genetics. *Ophthalmology.* 2008;115:1632, 1632. e1. http://www.ophsource.org/periodicals/ophtha/article/S0161-6420(08)00226-1/. Accessed March 29, 2012.
28. Nakanishi H, Gotoh N, Yamada R, et al. ARMS2/HTRA1 and CFH polymorphisms are not associated with choroidal neovascularization in highly myopic eyes of the elderly Japanese population. *Eye (Lond).* 2010;24:1078–1084.
29. Seo MS, Kwak N, Ozaki H, et al. Dramatic inhibition of retinal and choroidal neovascularization by oral administration of a kinase inhibitor. *Am J Pathol.* 1999;154:1743–1753.
30. Kwak N, Okamoto N, Wood JM, Campochiaro PA. VEGF is major stimulator in model of choroidal neovascularization. *Invest Ophthalmol Vis Sci.* 2000;41:3158–3164.
31. Krzystolik MG, Afshari MA, Adamis AP, et al. Prevention of experimental choroidal neovascularization with intravitreal anti-vascular endothelial growth factor antibody fragment. *Arch Ophthalmol.* 2002;120:338–346.
32. Ishida S, Yamashiro K, Usui T, et al. Leukocytes mediate retinal vascular remodeling during development and vaso-obliteration in disease. *Nat Med.* 2003;9:781–788.
33. Ishida S, Usui T, Yamashiro K, et al. VEGF164-mediated inflammation is required for pathological, but not physiological, ischemia-induced retinal neovascularization. *J Exp Med.* 2003;198:483–489.
34. Bates DO, Cui TG, Doughty JM, et al. VEGF165b, an inhibitory splice variant of vascular endothelial growth factor, is down-regulated in renal cell carcinoma. *Cancer Res.* 2002;62:4123–4131.
35. The International HapMap Project. International HapMap Consortium. *Nature.* 2003;426:789–796.

Automated Assessment of Drusen Using Three-Dimensional Spectral-Domain Optical Coherence Tomography

Daisuke Iwama,[1] Masanori Hangai,[1] Sotaro Ooto,[1] Atsushi Sakamoto,[1] Hideo Nakanishi,[1] Takashi Fujimura,[2] Amitha Domalpally,[3] Ronald P. Danis,[3] and Nagahisa Yoshimura[1]

Purpose. To compare automated assessment of macular drusen delineated by the authors' originally developed algorithm on three-dimensional (3D) spectral-domain optical coherence tomography (SD-OCT) with the assessment by certified graders on color fundus photographs in nonneovascular age-related macular degeneration (AMD).

Methods. Automated assessment of macular drusen was performed using raster scan by 3D OCT scans in 18 eyes with nonneovascular AMD with at least one large druse (≥125 μm) and predominantly soft indistinct drusen. Drusen was defined as the regions that have the distance between the retinal pigment epithelium and calculated Bruch's membrane lines > predefined threshold distances. The agreement was assessed on maximum drusen size and drusen area within grid between 3D SD-OCT and color fundus photographs, and false-negative and false-positive drusen at each threshold distance.

Results. There was agreement or agreement within one step in all eyes in maximum drusen size, and 15 (83.3%) of the eyes in the drusen area, except 6 pixels, regardless of threshold distances. However, the number of eyes with exact agreement in the drusen area increased when the threshold distances were smaller than 4 pixels. In the three cases with disagreement in the drusen area, false-negative drusen on 3D SD-OCT were characterized by being small in area and height.

Conclusions. Automated assessment of drusen parameters based on the authors' algorithm on 3D SD-OCT, which was limited by the poor detection ability of small drusen, showed good agreement with the assessment by certified graders on color fundus photography in these subjects. (*Invest Ophthalmol Vis Sci.* 2012;53:1576-1583) DOI:10.1167/iovs.11-8103

From the [1]Department of Ophthalmology and Visual Sciences, Kyoto University Graduate School of Medicine, Kyoto, Japan; [2]Topcon Corporation, Tokyo, Japan; and the [3]Fundus Photograph Reading Center, Department of Ophthalmology and Visual Sciences, University of Wisconsin, Madison, Wisconsin.

Supported in part by Grant-in-Aid for Scientific Research 21249084, Japan Society for the Promotion of Science, Tokyo, Japan; and the Japanese National Society for the Prevention of Blindness.

Submitted for publication June 22, 2011; revised October 30 and December 24, 2011; accepted January 21, 2012.

Disclosure: **D. Iwama**, None; **M. Hangai**, Topcon Corp. (C), Nidek Co. Ltd. (C); **S. Ooto**, None; **A. Sakamoto**, None; **H. Nakanishi**, None; **T. Fujimura**, Topcon Corp. (E); **A. Domalpally**, None; **R.P. Danis**, GSK (C), CoMentis (C), Sangamo (C); **N. Yoshimura**, Topcon Corp. (C), Nidek Co. Ltd. (C)

Corresponding author: Masanori Hangai, Department of Ophthalmology and Visual Sciences, Kyoto University Graduate School of Medicine, 54 Kawahara-cho, Shougoin, Sakyo-ku, Kyoto 606-8507, Japan; hangai@kuhp.kyoto-u.ac.jp.

Drusen are extracellular deposits that accumulate between the retinal pigment epithelium (RPE) and the inner collagenous layer of Bruch's membrane, resulting in anteriorly protruding RPE over the straight Bruch's membrane.[1] Drusen are a distinguishing feature of nonneovascular age-related macular degeneration (AMD). The parameters for estimating drusen, such as total drusen area and maximum drusen size in the macula, have been shown to have correlations with risk of progression to advanced AMD.[2-8] The Age-Related Eye Disease Study (AREDS) reported that by taking a high dose vitamin and mineral supplement, AMD patients with advanced dry AMD or vision loss resulting from neovascular AMD in one eye or extensive intermediate size drusen (at least one large druse), or noncentral geographic atrophy in both eyes could delay the onset of severe AMD and accompanying severe vision loss.[9] This constitutes important evidence, suggesting that earlier identification of the patients at higher risk for advanced AMD allows earlier protective intervention to reduce severe vision loss. Thus, it is becoming more important to assess changes in drusen and the RPE morphology to monitor the progression of nonneovascular AMD.

Assessment of drusen on color fundus photography may be performed according to the grading protocols established by Wisconsin Reading Center as widely used in epidemiologic studies and adapted for clinical trials, such as the AREDS.[10-12] However, the assessment of drusen on color fundus photography is effort intensive, often used with a multigrader methodology for achieving objective assessment.

Optical coherence tomography (OCT) is an interferometric technology for in vivo high-resolution, cross-sectional imaging of ocular structures, which allows automated and objective measurement of retinal structures.[13] Recently developed spectral-domain OCT (SD-OCT) technology allows much faster imaging (43 to 133 times faster than originally developed time-domain OCT [TD-OCT] technology), and three-dimensional (3D) analysis of macular pathologies.[14-17] High-speed OCT imaging allows the elimination of eye motions in B-scans, therefore creating OCT images that better reflect the true retinal geometry than does TD-OCT, which cannot reliably reproduce the shape of the RPE. High-speed OCT imaging also enables dense 3D raster scanning, which theoretically allows detection of drusen that are small in size. Commercially available SD-OCT instruments have twice higher axial resolution (5-7 μm) than Stratus OCT. Higher axial resolution theoretically allows improved visualization of drusen that are small in height. Thus, SD-OCT instruments potentially allow depiction of small drusen.

Recent studies showed the potential advantages of SD-OCT in assessing drusen, such as manual measurement of drusen volume[18]; semiautomatic measurement of drusen area and drusen size[19,20]; automatic detection and measurement of drusen area, height, and volume[21-23]; improved visualization of

Investigative Ophthalmology & Visual Science, March 2012, Vol. 53, No. 3
Copyright 2012 The Association for Research in Vision and Ophthalmology, Inc.

drusen ultrastructures[24]; and assessment of damages of photoreceptor layer over drusen.[25] Most recent studies also showed that the assessment of drusen using SD-OCT was applicable for monitoring drusen changes in volume and area over time[26] and for assessing drusen in eyes with drusen and geographic atrophy.[27] However, no previous studies reported the correlation of the automatically measured drusen parameters, such as drusen area and maximum drusen size, with those assessed by the gold standard drusen assessment within the Early Treatment of Diabetic Retinopathy Study (ETDRS) grid chart (6 mm) on color fundus photography. The purpose of this study was to compare automated drusen assessment using an originally developed algorithm on SD-OCT (3D OCT-1000; Topcon, Tokyo, Japan) imaging with the results by certified graders using the AREDS drusen grading system from color fundus photography.

Methods

We prospectively examined 22 patients (22 eyes) with soft drusen who were referred to the Macula Service of the Department of Ophthalmology, Kyoto University Hospital, from January 2008 through November 2008. For inclusion in this study, subjects had a clinical diagnosis of AREDS Category 3 nonneovascular AMD with at least one large druse (diameter $\geq$ 125 μm) in the macula of the eye under study.[10] Eyes with noncentral geographic atrophy (GA) were excluded. Eyes with ocular media opacity affecting fundus imaging were excluded from the study. Eyes with other macular abnormalities or any other condition that could cause RPE abnormalities unrelated to soft drusen were excluded.

All patients had a comprehensive ophthalmologic examination, using the 3D OCT scans (OCT-1000) and single-field nonstereoscopic digital color fundus photographs obtained with the 3D scans (OCT-1000). All investigations of this study adhered to the tenets of the Declaration of Helsinki. This study was approved by the Institutional Review Board and Ethics Committee of the Kyoto University Graduate School of Medicine. Informed consent was obtained for all patients.

Photographic Drusen Area Grading by Wisconsin Graders

Drusen classification from nonstereo single-field digital color fundus photographs was performed by graders using the AREDS grading protocol, with modification to account for use of a single-field digital image.[10-12] Maximum drusen size and drusen area within the ETDRS grid were evaluated by certified graders at the Fundus Photograph Reading Center at the University of Wisconsin for each subfield of ETDRS grid charts (Fig. 1), according to the Wisconsin grading system. In the current AREDS grading system, the diameter of the optic disc is estimated at 1800 μm compared with the 1500 μm in the original AREDS grading system; consequently, the diameter of the current ETDRS grid is 7200 μm. However, the current SD-OCT instruments do not permit 3D imaging in areas larger than 6.0 $\times$ 6.0-mm square area, which is smaller than the current ETDRS grid. In this study, we used the conventional 6000 μm ETDRS grid to compare drusen detection on 3D imaging with the AREDS grading system within the same area.

3D Macular Imaging with SD-OCT

A 6 $\times$ 6-mm area centered on the fovea was scanned with a standard raster-scan protocol (using the 3D OCT-1000), which included 128 sequential horizontal scans, each of which consisted of 512 axial scans with a depth of 1.68 mm. This protocol provides horizontal pixel spacings of 11.7 μm (6 mm/512 A-scans), vertical pixel spacings of 46.9 μm (6 mm/128 A-scans), and axial pixel spacing of 3.5 μm (1.68 mm/480 pixels). The image quality of the SD-OCT B-scan images that had an image quality index of >50 was used for analysis.

Automated Delineation of Macular Drusen with Optical Coherence Tomography

Definition of the Bruch's Membrane. Custom-made functions for automated delineation of macular drusen on the 3D raster scan data set (originally developed by Topcon) were based on built-in software (3D OCT-1000). We defined drusen on each SD-OCT B-scan image based on two segmented lines: the anterior boundary line of the RPE and the calculated line representing the presumed Bruch's membrane as the drusen floor. However, the reflectivity of the Bruch's membrane line is frequently weak or unseen beneath drusen, leading to segmentation errors.[18-25] In histopathologic specimens, Bruch's membrane remains as a straight line beneath the drusen elevating the RPE.[28,29] Thus, the presumed Bruch's membrane line beneath the drusen can be approximated by extrapolation from the visible line on either side of drusen.[20,22,23] In detail, B-scan images were binarized after processing with a median filter. Canny edge detection was used to determine the inner limiting membrane (ILM) line as a boundary from low to high reflectivity (positive edge) in the inner portion of the retina. Another positive edge below the ILM line was detected using the same method, as a photoreceptor inner and outer segment junction (IS/OS) line. The line with the highest reflectivity within 30 pixels (105 μm) below the IS/OS line was determined as the line representing the RPE. The RPE line was globally fitted with straight lines as follows. The lowest point of the segmented RPE line within the B-scan image frame was determined. The nearest point of tangency on the left side of the tangential straight line through the lowest point was determined. Then, another straight line through the nearest point of tangency was used to determine the second nearest point of tangency on the left side. The same process was repeated to the end of the left side. Fitting with straight lines on the right side was carried out in the same way. A quadratic curve along the anterior boundary of the healthy RPE line was calculated using the least-squares method as a calculated Bruch's membrane by referring the fitted straight lines where the distance between the segmented RPE line and fitted straight lines were within 3 pixels. We defined drusen as regions where the distance between the two delineated lines (RPE and Bruch's membrane) was greater than the defined minimal distance (see the following text).

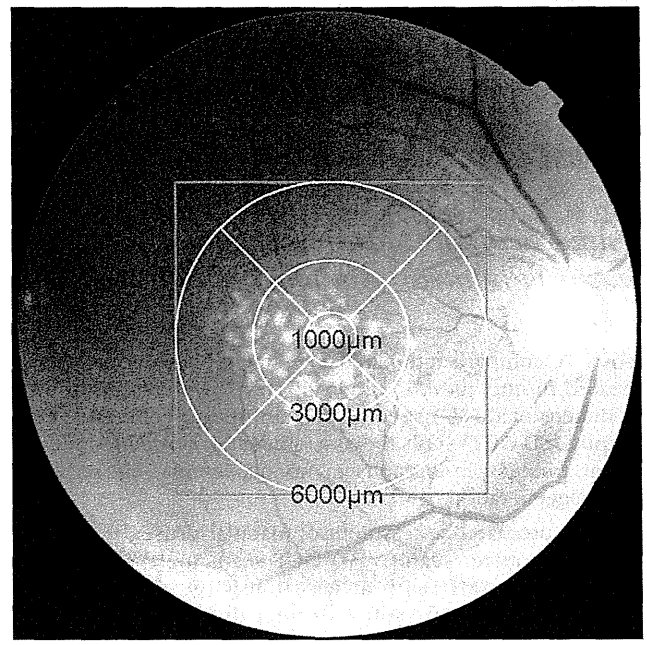

FIGURE 1. ETDRS grid charts used to define subfields in the macular area. Before grading, a grid consisting of three circles concentric with the center of the macula and four radial lines is superimposed over the fundus photograph. The radius of the innermost circle corresponds to 500 μm in the fundus photograph, and the radii of the middle and outer circles correspond to 1500 and 3000 μm, respectively. The length of the *green lines* for the outer square is 6000 μm, which is the area examined with 128 sequential horizontal SD-OCT scans in the present study.

Area Mapping of Drusen. OCT fundus images were created as an en face projection image from the SD-OCT data set by integrating the magnitudes of the OCT signals at each lateral position along the axial direction, as previously described.[17] The en face SD-OCT image was registered to that of color fundus photographs based on the retinal vessel patterns and the optic nerve head as landmarks. Color fundus photographic images were converted into monochromatic images and adjusted in size to the en face SD-OCT images. Next, we performed edge detection based on signal intensity for the en face SD-OCT images. Processing in this way provides characteristic high-contrast images, in which retinal vascular patterns are highlighted. Spatial correlations of vascular patterns between the processed en face SD-OCT images and monochromatic fundus photographs were calculated to determine the optimal agreement in location for both images. If there were apparent gaps between the two images, we manually face SD-OCT images. The delineated drusen area was mapped on each color fundus photograph with the ETDRS grid chart. The drusen area was obtained by 3D mapping of basal areas for the defined drusen that were determined in the 3D volume ("cube") scan. We did not manually correct segmentation errors on SD-OCT images for analysis of drusen size and area within the grid.

Determination of Optimal Threshold for Detecting Drusen on B-Scan Images. To find the optimal threshold distance for defining drusen, we calculated the maximum drusen size and drusen area within the grid by changing the threshold distances from 1 pixel to 6 pixels (1 pixel = 3.5 μm). The calculated maximum drusen size and drusen area within the grid on the 3D SD-OCT data set for each pixel category were compared with the results of the color fundus photograph grading. When the calculated values were within the range of the category determined by certified graders, we regarded this agreement as "agree." When they were within range of the neighboring category, we regarded the agreement as "agree within 1 step." When they were out of range of the determined category and its neighboring categories, we regarded the agreement as "disagree."

We also counted the number of false-positive drusen at each of the threshold distance categories (6 pixels to 1 pixel) by comparing results of the drusen mapping with the registered color fundus photographs as described in the following text.

Evaluation of Segmentation Algorithm Failure

All the segmentation algorithm outputs were subjectively evaluated independently by two experts (SO, AS), who were masked to other clinical information. We used criteria of segmentation algorithm failure originally used by Ishikawa et al.[30] In detail, algorithm failures were defined as an obvious disruption of the detected border, and/or border wandering (detected border jumping to and from different anatomic structures) for >5% consecutive (i.e., an uninterrupted error) or 20% cumulative (i.e., adding up all errors amounts to 20% of the image width) of the entire image.

Statistics

Numbers of false-negative and false-positive drusen among the threshold pixel categories were used to define drusen on SD-OCT images, and the number of automatically detected drusen among subfields of the grid were compared by Kruskal–Wallis test, with post hoc comparisons tested with the Dunnett's rank test. Percentages of agreement and correspondence exact and within one step, were calculated and unweighted and weighted kappa scores were computed to determine intergrader agreement.[31] Intraclass correlation coefficients (ICCs) were computed. Statistical software (Statview 5.0; SAS Institute, Cary, NC) was used for statistical analyses. A value of $P < 0.05$ was considered statistically significant.

Results

SD-OCT examinations were performed on 22 eyes of 22 Japanese patients with a clinical diagnosis of nonneovascular AMD with soft drusen. Four eyes were excluded because their quality index was <50. The remaining 18 eyes of 18 patients (13 males and 5 females) underwent analysis. These eyes, which had nonneovascular AMD with soft drusen, were found in the fellow eye of 18 patients with exudative AMD; thus, no patients met the inclusion criteria in both of their eyes. The patients were 66 to 90 years of age with a median of 78 years. The mean (±SD) spherical equivalent was −0.36 ± 1.6 (range, −3.25–1.5). The best-corrected visual acuity of the affected eyes ranged from 20/25 to 20/12.5 (median, 20/20 in Snellen equivalent).

Drusen Grading and Agreement on Color Fundus Photography

Table 1 demonstrates the characteristics of drusen according to conventional AREDS grading system on color photographs. There were definite, predominantly soft indistinct drusen in the macular area, except in one eye. The maximum drusen size was >300 μm except in one eye. Drusen area within the grid

Table 1. Characteristics of Drusen Graded by the Conventional AREDS Grading System

Subject Number	Maximum Drusen Size	Drusen Area within Grid	Soft Drusen within Grid	Drusenoid PED
1	≥ drusen circle C2	≥1 DA	Predominantly soft indistinct	Absent
2	≥ drusen circle C2	<1 DA	Predominantly soft indistinct	Absent
3	≥ drusen circle C2	<1 DA	Predominantly soft indistinct	Absent
4	< drusen circle C2	≥1 DA	Predominantly soft indistinct	Absent
5	≥ drusen circle C2	<1/2 DA	Predominantly soft indistinct	Absent
6	≥ drusen circle C2	<1/2 DA	soft indistinct present	Absent
7	≥ drusen circle C2	≥1 DA	Predominantly soft indistinct	Absent
8	≥ drusen circle C2	≥1 DA	Predominantly soft indistinct	Absent
9	≥ drusen circle C2	≥1 DA	Predominantly soft indistinct	Absent
10	≥ drusen circle C2	≥1 DA	Predominantly soft indistinct	Absent
11	≥ drusen circle C2	< drusen circle O2	Predominantly soft indistinct	Absent
12	≥ drusen circle C2	≥1 DA	Predominantly soft indistinct	Absent
13	≥ drusen circle C2	≥1 DA	Predominantly soft indistinct	Absent
14	≥ drusen circle C2	≥1 DA	Predominantly soft indistinct	Absent
15	≥ drusen circle C2	<1 DA	Predominantly soft indistinct	Absent
16	≥ drusen circle C2	≥1 DA	Predominantly soft indistinct	Absent
17	≥ drusen circle C2	≥1 DA	Predominantly soft indistinct	Absent
18	≥ drusen circle C2	≥1 DA	Predominantly soft indistinct	Absent

The drusen size measurements are based on the modern assumption. C2 = 300 μm; O2 = 790 μm; and 1 DA = 2.54 mm^2. DA, disc area; PED, pigment epithelial detachment.

TABLE 2. Maximum Drusen Size and Drusen Area within Grid Calculated on Various Threshold Distances on 3D Optical Coherence Tomography, and Their Agreement with Color Photograph Grading by the AREDS Grading System

Subject	Maximum Drusen Size (μm) on AGS	Maximum Drusen Size (μm) on SD-OCT: Number of Pixels Used to Define Drusen on SD-OCT					
		6	5	4	3	2	1
1	300 ≤	1818	1858	1914	1983	2037	2145
2	300 ≤	775	788	804	812	830	842
3	300 ≤	716	735	750	764	780	792
4	150 ≤, < 300	190	211	228	253	332	360
5	300 ≤	517	592	611	633	723	761
6	300 ≤	632	675	704	734	754	776
7	300 ≤	1416	1457	1525	1571	1648	1690
8	300 ≤	831	846	863	877	889	1042
9	300 ≤	1182	1247	1295	1352	1461	1512
10	300 ≤	2291	2341	2413	2594	2706	2779
11	300 ≤	392	436	461	485	507	527
12	300 ≤	679	934	1077	1117	1160	1217
13	300 ≤	787	832	878	914	1203	1235
14	300 ≤	955	987	1654	1738	1992	2204
15	300 ≤	316	337	499	537	563	591
16	300 ≤	419	452	482	511	539	572
17	300 ≤	1186	1218	1248	1282	1310	1336
18	300 ≤	2501	2540	2569	2594	2632	2670
Exact agreement		18	18	18	18	17	17
Agreement within 1 step		0	0	0	0	1	1
Disagreement		0	0	0	0	0	0

Subject	Drusen Area within Grid (%) on AGS	Drusen Area within Grid (%) on SD-OCT: Number of Pixels Used to Define Drusen on SD-OCT					
		6	5	4	3	2	1
1	8.9 ≤	13.03	14.13	15.17	16.33	17.46	18.76
2	4.5 ≤, < 8.9	2.15	2.32	2.51	2.80	3.19	3.50
3	4.5 ≤, < 8.9	2.28	2.75	3.29	4.02	4.87	5.68
4	8.9 ≤	0.33	0.53	0.87	1.44	2.21	2.97
5	1.7 ≤, < 4.5	1.76	1.92	2.13	2.41	2.67	2.96
6	1.7 ≤, < 4.5	1.16	1.29	1.43	1.74	1.97	2.25
7	8.9 ≤	6.81	7.51	8.32	9.05	9.81	10.65
8	8.9 ≤	9.22	10.30	11.56	12.95	14.64	16.40
9	8.9 ≤	6.05	7.29	8.60	10.26	11.93	14.14
10	8.9 ≤	28.92	31.36	34.22	37.33	40.80	44.69
11	<1.7	0.62	0.78	0.87	1.00	1.16	1.52
12	8.9 ≤	4.42	5.27	6.30	7.39	8.82	10.69
13	8.9 ≤	9.99	12.17	14.46	16.58	18.62	20.87
14	8.9 ≤	12.92	14.25	15.88	17.78	19.88	22.15
15	4.5 ≤, < 8.9	0.58	0.71	0.85	1.06	1.30	1.55
16	8.9 ≤	1.95	2.19	2.50	2.86	3.19	3.62
17	8.9 ≤	6.57	7.18	7.82	8.65	9.43	10.26
18	8.9 ≤	18.39	19.07	19.88	20.83	22.46	25.05
Exact agreement		8	8	8	11	13	14
Agreement within 1 step		6	7	7	4	2	1
Disagreement		4	3	3	3	3	3

AGS, Age-Related Eye Disease Study Grading System.

was categorized as grade 4 (<790 μm circle) in one eye, categorized as grade 5 (less than half of the disc area) in 2 eyes, categorized as grade 6 (from half to one disc area) in 3 eyes, and categorized as grade 7 (one disc area or more) in 12 eyes. Reproducibility was assessed by verification by a different grader. Agreement for maximum drusen size was 94% (κ = 0.64) and for drusen area within grid 83% (κ = 0.67).

Maximum Drusen Size and Drusen Area within Grid Calculated on Various Threshold Distances on 3D OCT

Maximum drusen size and drusen area within the grid were calculated for automatically delineated drusen on SD-OCT images based on various threshold distances (6 pixels to 1 pixel) in the definition of macular drusen (Table 2). Between the results of AREDS grading system and OCT, there was agreement or agreement within one step in all the 18 eyes in the maximum drusen size regardless of the threshold distances. With regard to drusen area within the grid, there was exact agreement or agreement within one step in 15 (83.3%) of 18 eyes regardless of the threshold distances except for 6 pixels (77.7%) as a threshold distance. In particular, exact agreement improved when the threshold algorithm used a distance smaller than 4 pixels.

When the threshold algorithm used a distance smaller than 4 pixels, grading results for maximum drusen size obtained by

Grader 1 showed exact agreement with those by OCT, whereas results by Grader 2 showed exact agreement with those by OCT in 17 (94.4%) of 18 eyes. For the drusen area, grading results obtained by Grader 1 showed exact agreement with those by OCT in 16 (88.9%) of 18 eyes, whereas results by Grader 2 showed exact agreement with those by OCT in 15 (83.3%) of 18 eyes.

For intersession reproducibility, ICC values for maximum drusen size and drusen area calculated in selected 10 eyes were 0.999 and 0.996, respectively.

Characteristics of Cases with Disagreement in the Drusen Area within the Grid

Three cases (cases 4, 15, and 16) showed consistent disagreement in the drusen area within the grid regardless of the threshold distances. The other eyes had varying size of drusen including confluent drusen (Fig. 2). Automated detection of drusen on SD-OCT imaging detected relatively large-sized drusen, including confluent drusen, but did not detect isolated drusen small in size on color fundus photographs. The drusen that were not detected by automated detection on SD-OCT images were characterized on SD-OCT images as being small in height (flattened) and as having a hyporeflective RPE line on the drusen. The three cases with consistent disagreement were characterized as having a large number of small drusen (Fig. 3). Even when we used smaller threshold distances, a large part of these small drusen were not detectable.

Segmentation Errors

Algorithm failure was detected in 2.95%, 2.99%, and 3.13% of total B-scan images (2304 images of 18 cases) by expert 1, expert 2, and both, respectively (Table 3). Expert assessment of algorithm failure showed almost perfect agreement between experts ($\kappa = 0.95$). The number of B-scan images with algorithm failures per eye ranged from 0 (0%) to 25 (19.5%) (mean ± SD = 3.8 ± 6.7 [3.0 ± 5.2%]).

Discussion

SD-OCT provides depth information at high axial resolution, allowing detection of fine abnormal elevations of the RPE in various pathologies, such as drusen,[18–23] pigment epithelial detachment,[32,33] and polypoidal lesions.[32] High-speed imaging in SD-OCT allows dense 3D imaging of these pathologic changes.[18–23] Automated drusen detection using 3D SD-OCT imaging may be a potentially useful alternative method to drusen assessment by human graders using color fundus photographs. Yi et al.[20] reported a preliminary study in which SD-OCT was shown to be able to determine the drusen area and drusen volume in a semiautomated manner, although the general applicability of their method remained unclear. Jain et al.[19] semiautomatically measured maximum drusen diameter and mean drusen area within a small macular area of 2 mm in diameter in subjects with AREDS Category 3 nonneovascular AMD and found good agreement of these parameters on SD-OCT with those identified on color fundus photographs. Gregori et al.[22] and Schlanitz et al.[23] were the first to demonstrate the completely automated detection of drusen. Gregori and colleagues[22] showed that SD-OCT allowed highly reproducible automated measurements of the drusen area and volume in subjects with nonneovascular AMD. Schlanitz and colleagues[23] showed that their automated segmentation algorithm, based on a new SD-OCT technology, polarization-sensitive OCT, identified 96.5% of all drusen without significant error in subjects with AREDS Category 2 or 3 nonneovascular AMD. Thus, agreement between such algorithms to automatically detect drusen and conventional grading of drusen on color fundus photography remained to be determined.

Drusen are features defined as abnormal appearances of the macular RPE on biomicroscopic examination and color fundus photography. It is currently unclear whether all the drusen determined on the basis of abnormal RPE geometry on OCT B-scans are actually drusen.[22] Abundant evidence regarding the

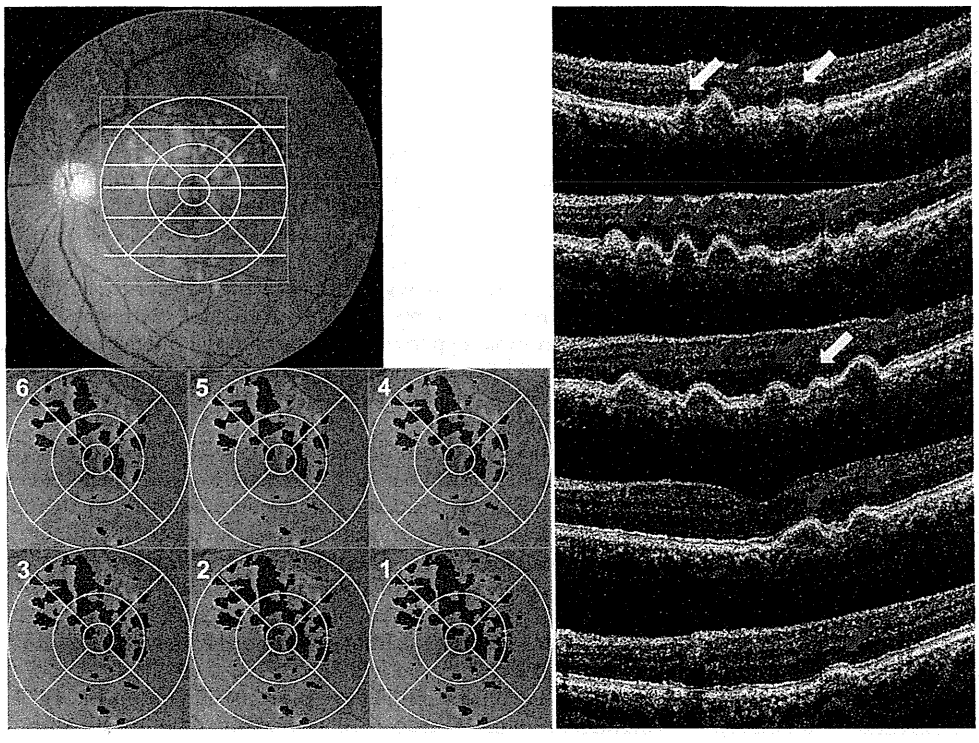

FIGURE 2. A representative case with exact agreement. An 81-year-old man (subject 14) who had exudative AMD in his right eye was found to have an asymptomatic, nonvascular AMD in the left eye. The visual acuity in the left eye was 20/12.5 in Snellen equivalent. (**A**) Color fundus photograph with ETDRS grid charts to define subfields of the macula. Soft drusen including a confluent soft drusen and small drusen were seen within the grid. (**B–F**) Five sectional images obtained by SD-OCT along *yellow lines* shown in (**A**). *Green lines* indicate automatically delineated anterior boundary of the RPE, which showed apparent protrusions of RPE that correspond to confluent soft drusen. *Blue lines* indicate the calculated Bruch's membrane lines. *Red arrows* point to the drusen automatically detected by our algorithm using 5 pixels as threshold height, and *yellow arrows* to drusen that were not detected. (**G–L**) Six small panels indicate the automatically delineated drusen area when 1, 2, 3, 4, 5, and 6 pixels were set as threshold height. The number in the *lower-left corner* in *each panel* indicates the number of pixels used for drusen definition. Drusen area was mapped in *blue* on the color fundus photographs. *Red* and *yellow arrows* (in **B–F**) point to the drusen indicated by *red* and *yellow arrows* (in **G–L**), respectively.

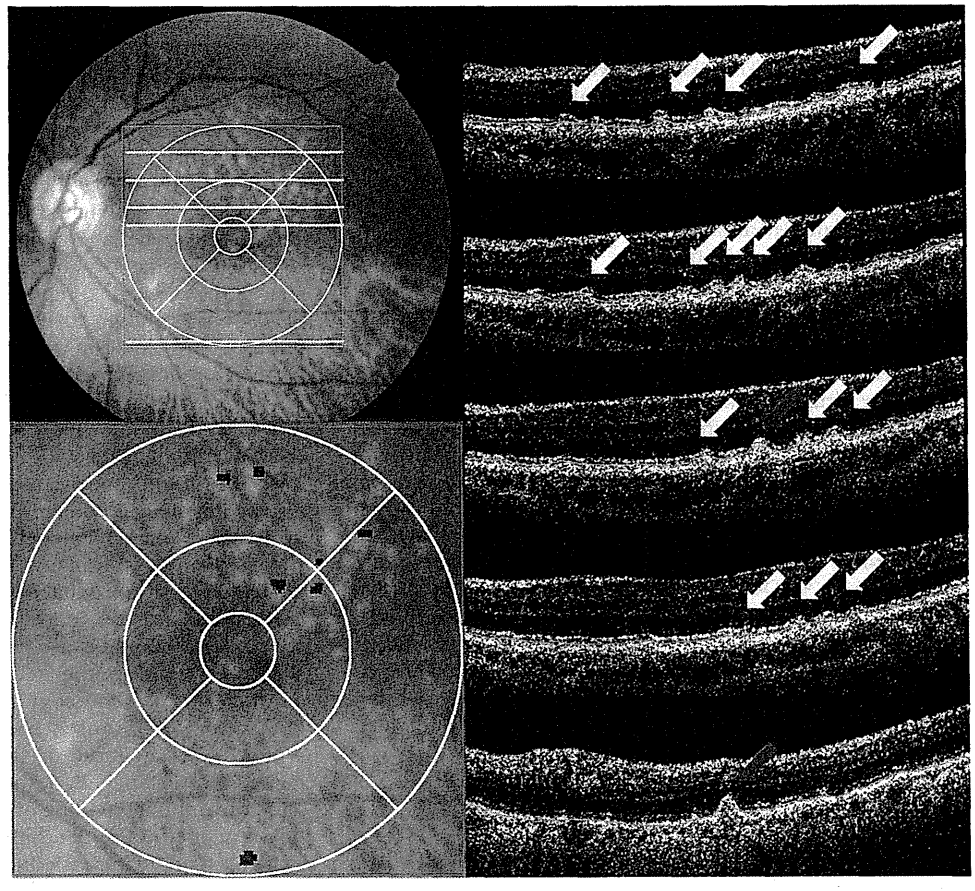

FIGURE 3. A representative case with disagreement. A 78-year-old man (subject 4) who had exudative AMD in his right eye was found to have an asymptomatic, nonvascular AMD in the left eye. The visual acuity in the left eye was 20/20 in Snellen equivalent. (**A**) Color fundus photograph with ETDRS grid charts to define subfields of the macula. There were many small drusen seen in the superior hemisphere of the grid. (**B–F**) Five sectional images obtained by SD-OCT along *yellow lines* shown in (**A**). *Green lines* indicate automatically delineated anterior boundary of the RPE. *Blue lines* indicate the calculated Bruch's membrane lines. The protrusions of RPE were mild except for those indicated by *red arrows*. *Red arrows* point to the drusen automatically detected by our algorithm using 5 pixels as threshold height, and *yellow arrows* to drusen that were not detected. (**G**) The automatically delineated drusen area using 5 pixels as threshold height was mapped in *blue* on the ETDRS grid charts and color fundus photographs. *Red* and *yellow arrows* in **B–F** point to the drusen indicated by *red* and *yellow arrows* in **G–L**, respectively.

clinical significance of drusen has accumulated based on photographic appearances of drusen; drusen parameters, such as total drusen area and maximum drusen size, categorized in accordance with the AREDS grading protocol on color fundus photographs, have been shown to have positive correlations with risks of progression to advanced AMD, and are now used as standard entry criteria and endpoints for disease progression in AMD clinical trials.[4–9] Thus, photographic appearances of drusen and their grading by certificated graders are the gold standards for implicating drusen in the risk for developing neovascular AMD. Since it is difficult to repeat previous key studies on a large scale, it is important to increase our understanding of the relationship between drusen categories on SD-OCT and color fundus photographs. The present study showed somewhat limited agreement in the drusen area between the drusen parameters measured using our automated drusen detection algorithms on conventional SD-OCT images and the drusen parameters graded by certified graders on color fundus photography.

We used an automated algorithm to detect drusen. Here, we used a simple method based on threshold height (= threshold distance between the inner boundary of the RPE and calculated Bruch's membrane) to define drusen. This automated segmentation method to delineate drusen is basically similar to the highly reproducible method reported by Gregori et al.[22] and the highly sensitive method reported by Schlanitz et al.,[23] in that the distance between the RPE and calculated Bruch's membrane lines (which they call interpolated RPE floor or RPE backbone) was used to delineate drusen. Successful (reproducible and accurate) performance of automated drusen detection using the threshold height depends on at least two important factors: reliable automated segmentation of the highly reflective RPE line[21–23] and the threshold level for discriminating between a significant deviation of the RPE line from the calculated Bruch's membrane line and the noise that accompanies any measurement technique.[22]

Reliable automated segmentation of the RPE line is influenced by retinal features frequently associated with drusen, such as abnormal hyperreflective lesions in the outer photoreceptor layer,[34,35] medium internal reflectivity,[25] RPE irregularities, and invisibility of Bruch's membrane.[36] These features could cause segmentation algorithm failures for drusen detection. Schlanitz et al.[21] demonstrated detection of drusen using several types of clinical SD-OCT instruments and concluded that the commercially available automated segmentation algorithms had distinct limitations for reliable identification of drusen, especially smaller drusen; the best detection rate of drusen with negligible errors was approximately 30% in the Cirrus (Carl Zeiss Meditec Inc., Dublin, CA) 200 × 200 scan pattern. In our study, algorithm failures appeared to be minimal when inspected by graders (2.95% and 2.99% for the two graders), based on the previously reported definition of segmentation errors.[30] However, it is difficult to compare our results with this previous report on segmentation errors since segmentation errors were previously defined per druse,

TABLE 3. Number of Images with Algorithm Failures Detected by Experts

	Number of Images with Algorithm Failures		
Total Images	**Expert 1**	**Expert 2**	**Both Experts**
2304 of 18 cases	69 (2.99)	68 (2.95)	72 (3.13)

Data are the number of images, with the percentage of total images in parentheses.

whereas we calculated segmentation errors per B-scan. In addition, the definitions of segmentation error are different.

Previous studies using semiautomated or manual segmentation methods to delineate drusen on SD-OCT imaging have compared the results obtained with drusen assessment on color fundus photographs.[18,19] Jain et al.[19] compared drusen parameters between drusen segmented on SD-OCT and drusen delineated on color fundus photographs within a macular area of approximately 2 mm in diameter, centered on the fovea. Their method first identified suspected drusen areas based on irregularities in the automatically delineated RPE contour. They then made several manual adjustments to the suspected drusen areas, including adjustment of the lateral extent of marked drusen to correspond to the point at which the RPE deflection returned to baseline, and manual correction of segmentation errors. Freeman et al.[18] used manual segmentation of drusen on 96 SD-OCT images to determine drusen volumes. Although it is difficult to directly compare the results of these previous studies with those of our studies, these results showed good agreement or significant correlations with drusen assessment on color fundus photographs.

It was difficult to automatically detect isolated and small drusen using our automated detection algorithms on SD-OCT images. This is consistent with the previous study that showed a trend for less detection of smaller drusen by semiautomated and automated drusen assessment using SD-OCT compared with that using color fundus photographs.[19,21,22] Thus, the failure to detect some small drusen appears to be a common problem in automated drusen detection using RPE segmentation algorithms on SD-OCT images. This failure may be attributable to both the characteristics of the undetectable drusen and RPE segmentation errors.[21,22] Flat drusen may also go undetected due to the threshold used by the algorithms.[22] In our study, three cases (cases 4, 15, and 16) showed consistent disagreement in the drusen area within the grid, regardless of the threshold distances. Both of them had similar characteristic drusen patterns on color fundus photographs; these eyes included many small drusen. The undetectable drusen were also characterized as being small in height on OCT B-scan images. Failure to detect small drusen would have some effects on results in many patients, according to the AREDS Report No. 17: 1249 of 3212 participants (38.9%) in the study had only small drusen in their right eye, and 1096 (88%) of the participants had an area less than C-1 (<125 μm).[7] It has been well demonstrated that larger drusen are associated with a higher risk of developing neovascular AMD.[2–8] However, a larger amount of drusen increases the drusen area within the grid. It remains to be determined whether this limitation is acceptable.

The threshold height for discriminating between a significant deviation of the RPE line from the calculated Bruch's membrane line and the noise that accompanies any measurement technique remains unknown.[22] In the present study, we tested agreement with photographic grading results (the drusen gold standard) by changing the threshold height values. We found that there were few differences in the number of eyes with disagreement in the drusen area within the grid even if the number of pixels for definition changed. This is probably because decreasing the threshold height in our algorithm was not sufficient for improving the detection of the small drusen. Thus, this disagreement appears to indicate the limitation of our algorithm.

It is difficult to completely compare grading on color fundus photography and quantitative drusen assessment using SD-OCT because the former reduces the continuous drusen property into simple categorical data. Our comparison means that we reduced the quantitative drusen property measured with SD-OCT imaging into categorical data. Such a coarse scale, with only three groups for drusen size and four groups for drusen area, can cause more agreement between drusen parameters measured using SD-OCT images and color fundus photographs. We also included the neighboring category (agreement within one step), as a category other than disagreement.

In clinical practice, patients who have drusen are usually aged and often have media opacity due to cataracts. Greater media opacity often causes poorer OCT B-scan signal strength, which leads to unreliable measurements; lower signal strength is associated with decreased thickness of the macula and retinal nerve fiber layer (RNFL), as suggested by previous studies.[37,38] Cataract surgery increases both signal strength and RNFL thickness.[38] This could also be the case for drusen assessment, since our method to detect drusen is based on the segmentation of the anterior boundary of the RPE line, similar to measurement of thickness between two boundaries. Therefore, we used eyes with good B-scan images that had an image quality (signal strength) index of >50 for analysis.

SD-OCT may be complementary to the grading of color photographs for drusen; definition of drusen on color fundus photographs is based on macular pigment abnormalities, whereas on SD-OCT images it is based on abnormal RPE geometry.[22] The clinical significance of drusen detected only on SD-OCT images remains unknown. In addition, SD-OCT imaging can provide new drusen parameters, such as their height and volume of drusen,[18–20,22,23] drusen ultrastructure,[25] and abnormalities of outer retinal layers over drusen.[28] Longitudinal studies are required to determine the relationship between drusen detectable only on SD-OCT and novel drusen parameters visualized by SD-OCT with disease progression in AMD.

Theoretically, the algorithm that we used for determination of the presumed Bruch's membrane beneath drusen may have an inaccurate approximation of retinal geometry by a quadratic curve when B-scans include unusual retinal configurations, which may occur in eyes with high myopia. However, we did not encounter such issues for the determination of the presumed Bruch's membrane, probably because our subjects did not have high myopia.

The limitations of this study are small sample size and the bias present in study subject selection. Subjects were limited to those with nonneovascular AMD and at least one large druse ($\geq$125 μm) (AREDS Category 3 nonneovascular AMD); these subjects had predominantly soft indistinct drusen. We focused only on AREDS Category 3 nonneovascular AMD because eyes with AREDS Category 3 nonneovascular AMD have a much increased risk of progression to neovascular AMD.[39] The bias in study subject selection may have caused higher agreement than was actually present, because in clinical practice, some patients have only small drusen that can go undetected by our algorithms. Another limitation of this study is the use of a specific algorithm on a single type of SD-OCT instrument with one specific imaging protocol. The reproducibility and accuracy of drusen detection will differ with algorithm used, imaging protocols, and the type of instruments used. A third limitation of this study was that we used the conventional ETDRS grid with a diameter of 6000 μm. This is because the 3D imaging in the current SD-OCT instrument we used did not include a circle area wider than 6000 μm. However, we found similar agreement with the AREDS grading results on the new ETDRS grid with a diameter of 7200 μm regardless of the differences in the grid area (Iwama D, Hangai M, Yoshimura N, unpublished data, 2011). The development of SD-OCT instruments that allow wider 3D imaging would resolve this limitation.

Although limited to our particular algorithm for the detection of drusen, and to study subjects with AREDS Category 3 nonneovascular AMD and predominantly soft indistinct drusen, our study successfully showed that SD-OCT allowed automated assessment of drusen area and size based on the threshold distances

of the delineated RPE and calculated Bruch's membrane, with minimal segmentation algorithm failures, in good agreement with the categorized drusen parameters assessed by certified graders according to the established AREDS grading protocols on color fundus photography. The advantages of this method as a tool for evaluating drusen remain to be determined in a longitudinal study.

References

1. Abdelsalam A, Del Priore L, Zarbin MA. Drusen in age-related macular degeneration: pathogenesis, natural course, and laser photocoagulation-induced regression. *Surv Ophthalmol.* 1999; 44:1-29.
2. Pauleikhoff D, Barondes MJ, Minassian D, Chisholm IH, Bird AC. Drusen as risk factors in age-related macular disease. *Am J Ophthalmol.* 1990;109:38-43.
3. Bressler SB, Maguire MG, Bressler NM, Fine SL. Relationship of drusen and abnormalities of the retinal pigment epithelium to the prognosis of neovascular macular degeneration. The Macular Photocoagulation Study Group. *Arch Ophthalmol.* 1990;108:1442-1447.
4. Klein R, Klein BE, Tomany SC, Meuer SM, Huang GH. Ten-year incidence and progression of age-related maculopathy: the Beaver Dam eye study. *Ophthalmology.* 2002;109:1767-1779.
5. Wang JJ, Foran S, Smith W, Mitchell P. Risk of age-related macular degeneration in eyes with macular drusen or hyperpigmentation: the Blue Mountains Eye Study cohort. *Arch Ophthalmol.* 2003;121: 658-663.
6. van Leeuwen R, Klaver CC, Vingerling JR, Hofman A, de Jong PT. The risk and natural course of age-related maculopathy: follow-up at 6 1/2 years in the Rotterdam study. *Arch Ophthalmol.* 2003; 121:519-526.
7. Davis MD, Gangnon RE, Lee LY, et al. The Age-Related Eye Disease Study severity scale for age-related macular degeneration: AREDS Report No. 17. *Arch Ophthalmol.* 2005;123:1484-1498.
8. Mitchell P, Smith W, Attebo K, Wang JJ. Prevalence of age-related maculopathy in Australia. The Blue Mountains Eye Study. *Ophthalmology.* 1995;102:1450-1460.
9. A randomized, placebo-controlled, clinical trial of high-dose supplementation with vitamins C and E, beta carotene, and zinc for age-related macular degeneration and vision loss: AREDS Report No. 8. *Arch Ophthalmol.* 2001;119:1417-1436.
10. Klein R, Davis MD, Magli YL, Segal P, Klein BE, Hubbard L. The Wisconsin age-related maculopathy grading system. *Ophthalmology.* 1991;98:1128-1134.
11. The Age-Related Eye Disease Study system for classifying age-related macular degeneration from stereoscopic color fundus photographs: the Age-Related Eye Disease Study Report Number 6. *Am J Ophthalmol.* 2001;132:668-681.
12. Bird AC, Bressler NM, Bressler SB, et al. An international classification and grading system for age-related maculopathy and age-related macular degeneration. The International ARM Epidemiological Study Group. *Surv Ophthalmol.* 1995;39:367-374.
13. Hee MR, Baumal CR, Puliafito CA, et al. Optical coherence tomography of age-related macular degeneration and choroidal neovascularization. *Ophthalmology.* 1996;103:1260-1270.
14. Schmidt-Erfurth U, Leitgeb RA, Michels S, et al. Three-dimensional ultrahigh-resolution optical coherence tomography of macular diseases. *Invest Ophthalmol Vis Sci.* 2005;46:3393-3402.
15. Wojtkowski M, Srinivasan V, Fujimoto JG, et al. Three-dimensional retinal imaging with high-speed ultrahigh-resolution optical coherence tomography. *Ophthalmology.* 2005;112:1734-1746.
16. Srinivasan VJ, Wojtkowski M, Witkin AJ, et al. High-definition and 3-dimensional imaging of macular pathologies with high-speed ultrahigh-resolution optical coherence tomography. *Ophthalmology.* 2006;113:2054.e1-2054.14.
17. Hangai M, Ojima Y, Gotoh N, et al. Three-dimensional imaging of macular holes with high-speed optical coherence tomography. *Ophthalmology.* 2007;114:763-773.
18. Freeman SR, Kozak I, Cheng L, et al. Optical coherence tomography-raster scanning and manual segmentation in determining drusen volume in age-related macular degeneration. *Retina.* 2009; 30:431-435.
19. Jain N, Farsiu S, Khanifar AA, et al. Quantitative comparison of drusen segmented on SD OCT versus drusen delineated on color fundus photographs. *Invest Ophthalmol Vis Sci.* 2010;51:4875-4883.
20. Yi K, Mujat M, Park BH, et al. Spectral domain optical coherence tomography for quantitative evaluation of drusen and associated structural changes in non-neovascular age-related macular degeneration. *Br J Ophthalmol.* 2009;93:176-181.
21. Schlanitz FG, Ahlers C, Sacu S, et al. Performance of drusen detection by spectral-domain optical coherence tomography. *Invest Ophthalmol Vis Sci.* 2010;51:6715-6721.
22. Gregori G, Wang F, Rosenfeld PJ, et al. Spectral domain optical coherence tomography imaging of drusen in nonexudative age-related macular degeneration. *Ophthalmology.* 2011;118:1373-1379.
23. Schlanitz FG, Baumann B, Spalek T, et al. Performance of automated drusen detection by polarization-sensitive optical coherence tomography. *Invest Ophthalmol Vis Sci.* 2011;52:4571-4579.
24. Khanifar AA, Koreishi AF, Izatt JA, Toth CA. Drusen ultrastructure imaging with spectral domain optical coherence tomography in age-related macular degeneration. *Ophthalmology.* 2008;115: 1883-1890.
25. Schuman SG, Koreishi AF, Farsiu S, Jung SH, Izatt JA, Toth CA. Photoreceptor layer thinning over drusen in eyes with age-related macular degeneration imaged in vivo with spectral-domain optical coherence tomography. *Ophthalmology.* 2009;116:488-496.
26. Yehoshua Z, Wang F, Rosenfeld PJ, et al. Natural history of drusen in age-related macular degeneration using spectral domain optical coherence tomography. *Ophthalmology.* 2011;118:2434-2441.
27. Chiu SJ, Izatt JA, O'Connell RV, Winter KP, Toth CA, Farsiu S. Validated automatic segmentation of AMD pathology including drusen and geographic atrophy in SD-OCT images. *Invest Ophthalmol Vis Sci.* 2012;53:53-61.
28. Green WR, McDonnell PJ, Yeo JH. Pathologic features of senile macular degeneration. *Ophthalmology.* 1985;92:615-627.
29. Gass JDM. Diseases causing choroidal exudative and hemorrhagic localized (disciform) detachment of the retina and retinal pigment epithelium. In: Gass JDM, ed. *Stereoscopic Atlas of Macular Diseases: Diagnosis and Treatment.* 4th ed. St. Louis, MO: Mosby; 1997:49-145.
30. Ishikawa H, Stein DM, Wollstein G, Beaton S, Fujimoto JG, Schuman JS. Macular segmentation with optical coherence tomography. *Invest Ophthalmol Vis Sci.* 2005;46:2012-2017.
31. Landis JR, Koch GG. The measurement of observer agreement for categorical data. *Biometrics.* 1977;33:159-174.
32. Ojima Y, Hangai M, Sakamoto A, et al. Improved visualization of polypoidal choroidal vasculopathy lesions using spectral-domain optical coherence tomography. *Retina.* 2009;29:52-59.
33. Spaide RF. Enhanced depth imaging optical coherence tomography of retinal pigment epithelial detachment in age-related macular degeneration. *Am J Ophthalmol.* 2009;147:644-652.
34. Curcio CA, Medeiros NE, Millican CL. Photoreceptor loss in age-related macular degeneration. *Invest Ophthalmol Vis Sci.* 1996; 37:1236-1249.
35. Johnson PT, Brown MN, Pulliam BC, Anderson DH, Johnson LV. Synaptic pathology, altered gene expression, and degeneration in photoreceptors impacted by drusen. *Invest Ophthalmol Vis Sci.* 2005;46:4788-4795.
36. Chen Y, Vuong LN, Liu J, et al. Three-dimensional ultrahigh resolution optical coherence tomography imaging of age-related macular degeneration. *Opt Express.* 2009;17:4046-4060.
37. Cheung CY, Leung CK, Lin D, Pang CP, Lam DS. Relationship between retinal nerve fiber layer measurement and signal strength in optical coherence tomography. *Ophthalmology.* 2008;115: 1347-1351.
38. Mwanza JC, Bhorade AM, Sekhon N, et al. Effect of cataract and its removal on signal strength and peripapillary retinal nerve fiber layer optical coherence tomography measurements. *J Glaucoma.* 2011;20:37-43.
39. Ferris FL, Davis MD, Clemons TE, et al. A simplified severity scale for age-related macular degeneration: AREDS Report No. 18. *Arch Ophthalmol.* 2005;123:1570-1574.

Choroidal Thickness, Vascular Hyperpermeability, and Complement Factor H in Age-Related Macular Degeneration and Polypoidal Choroidal Vasculopathy

Pichai Jirarattanasopa,[1,2] *Sotaro Ooto,*[1] *Isao Nakata,*[1] *Akitaka Tsujikawa,*[1] *Kenji Yamashiro,*[1] *Akio Oishi,*[1] *and Nagahisa Yoshimura*[1]

Purpose. To investigate the relationship between subfoveal choroidal thickness, choroidal vascular hyperpermeability, and complement factor H (*CFH*) gene polymorphism in typical age-related macular degeneration (AMD) and polypoidal choroidal vasculopathy (PCV).

Methods. Fifty-eight patients with typical AMD and 63 patients with PCV underwent fluorescein angiography, indocyanine green angiography (IA), and spectral-domain optical coherence tomography (OCT) using enhanced depth imaging (EDI). Subfoveal choroidal thickness was measured using EDI-OCT images, and choroidal hyperpermeability was evaluated using late-phase IA images. The major AMD-associated single-nucleotide polymorphisms were genotyped in 86 patients.

Results. Mean subfoveal choroidal thickness was significantly lower in eyes with typical AMD than that in eyes with PCV ($P = 0.025$). Subfoveal choroidal thickness was greater in eyes with choroidal hyperpermeability than that in eyes without it in typical AMD ($P < 0.001$) and PCV ($P = 0.020$), and in the fellow eyes of typical AMD ($P < 0.001$) and PCV ($P = 0.027$). In eyes without choroidal hyperpermeability, the mean subfoveal choroidal thickness was greater in PCV than that in typical AMD ($P = 0.001$). Choroidal thickness decreased after photodynamic therapy combined with intravitreal ranibizumab in typical AMD ($P = 0.016$) and PCV ($P = 0.036$). In eyes with PCV, the I62V polymorphism in the *CFH* gene contributed to choroidal thickness ($P = 0.043$).

Conclusions. Choroidal thickness is related to the AMD subtypes, choroidal hyperpermeability, and I62V *CFH* gene polymorphism. In eyes without choroidal hyperpermeability, EDI-OCT is useful as an auxiliary measure for differentiating typical AMD and PCV. (*Invest Ophthalmol Vis Sci.* 2012; 53:3663-3672) DOI:10.1167/iovs.12-9619

Exudative age-related macular degeneration (AMD) is the leading cause of severe impairment of visual function in people older than 50 years of age who reside in industrialized countries. Maruko et al.[1] surveyed the distribution of exudative AMD subtypes in a Japanese population and showed that 35% of patients had typical AMD and 55% had polypoidal choroidal vasculopathy (PCV), which is characterized by orange subretinal polypoidal dilations arising from the choroidal vascular network.[2] Although verteporfin photodynamic therapy (PDT) tends to be of benefit in PCV,[3] antivascular endothelial growth factor (VEGF) therapy does not appear to diminish the polypoidal lesions.[4-6] In contrast, in eyes with typical AMD, anti-VEGF therapy provides greater clinical benefit than PDT.[7]

Indocyanine angiography (IA) has improved our knowledge of many macular diseases including typical AMD and PCV.[8-14] Choroidal vascular hyperpermeability is frequently seen in eyes with central serous chorioretinopathy,[8-11,14] but it is also seen in PCV and typical AMD,[13] suggesting that choroidal vascular abnormalities may be involved in the pathogenesis of these diseases. Since Spaide and colleagues[15] introduced enhanced depth imaging optical coherence tomography (EDI-OCT), an increasing number of investigators have studied choroidal thickness in healthy and diseased eyes.[16-26] Recently, several researchers have reported that subfoveal choroidal thickness is greater in eyes with PCV than that in eyes with typical AMD,[22-24] suggesting the involvement of different pathogenic mechanisms in typical AMD and PCV. However, little is known about the relationship between choroidal thickness, angiographic changes, and genetic background in these eyes.

In this study, we investigated a consecutive series of treatment-naïve patients with typical AMD and PCV to evaluate the relationship between the choroidal thickness on EDI-OCT, choroidal vascular hyperpermeability on IA, and major AMD-associated single nucleotide polymorphisms (SNPs; polymorphisms in the complement factor H [*CFH*] and age-related maculopathy susceptibility 2 [*ARMS2*] genes) in these two disorders.

Methods

All investigations adhered to the tenets of the Declaration of Helsinki, and the study was approved by the institutional review board and the ethics committee at Kyoto University Graduate School of Medicine. The nature of the study and its possible consequences were explained to the study candidates, after which written informed consent was obtained from all patients who were genotyped.

Subjects

We retrospectively reviewed medical charts of 121 consecutive treatment-naïve patients (58 patients with typical AMD and 63 patients with PCV) who visited the Macular Service at Kyoto University Hospital, Kyoto, Japan, between April 2009 and October 2011. All patients with typical AMD and PCV underwent best-corrected visual acuity (BCVA),

From the [1]Department of Ophthalmology and Visual Sciences, Kyoto University Graduate School of Medicine, Kyoto, Japan; and the [2]Department of Ophthalmology, Faculty of Medicine, Prince of Songkla University, Songkhla, Thailand.

Submitted for publication February 2, 2012; revised April 25, 2012; accepted April 25, 2012.

Disclosure: **P. Jirarattanasopa**, None; **S. Ooto**, None; **I. Nakata**, None; **A. Tsujikawa**, None; **K. Yamashiro**, None; **A. Oishi**, None; **N. Yoshimura**, None

Corresponding author: Sotaro Ooto, Department of Ophthalmology and Visual Sciences, Kyoto University Graduate School of Medicine, 54 Kawahara-cho, Shogoin, Sakyo-ku, Kyoto 606-8507, Japan; ohoto@kuhp.kyoto-u.ac.jp.

Copyright 2012 The Association for Research in Vision and Ophthalmology, Inc.

intraocular pressure, autorefractometry/keratometry, indirect ophthalmoscopy, slit-lamp biomicroscopy with a contact lens, color fundus photography, fluorescein angiography (FA), IA using a confocal laser scanning ophthalmoscope (HRA2; Heidelberg Engineering GmbH, Dossenheim, Germany), and spectral-domain (SD)-OCT (Spectralis; Heidelberg Engineering) using an EDI technique at baseline.

Diagnoses of typical AMD and PCV were based on the results of fundus examination, FA, IA, and OCT. Typical AMD was diagnosed in patients older than 50 years of age, with evidence of hyperfluorescence with late leakage on FA associated with pigment epithelium detachment (PED), serous retinal detachment (SRD), subretinal exudation, and hemorrhage in the macular region. PCV was diagnosed primarily on the basis of IA findings, branching vascular network, and terminating polypoidal lesions. All diagnoses were made by three retinal specialists (SO, KY, and AT); a fourth specialist (NY) was called on when the diagnosis could not be decided on by the initial three reviewers.

Exclusion criteria included the presence of high myopia with refractive error ≥ -6.0 diopters or axial length ≥ 26.5 mm; history of intraocular surgery including vitrectomy, cataract surgery (within 1 year before the measurement), anti-VEGF therapy, and PDT; history of ocular trauma; evidence of other retinal diseases including other neovascular maculopathy (i.e., retinal angiomatous proliferation, angioid streaks, idiopathic macular telangiectasia), glaucoma or high intraocular pressure (≥22 mm Hg); and poor image due to media opacity, thick subretinal hemorrhage, or unstable fixation. Subjects with systemic diseases or conditions such as diabetes mellitus or malignant hypertension that might affect choroidal thickness were also excluded.

Choroidal Hyperpermeability

Choroidal vascular hyperpermeability was evaluated in the late phase of IA, approximately 10–15 minutes after dye injection. According to the report by Guyer et al.,[8] choroidal vascular hyperpermeability was defined as multifocal areas of hyperfluorescence with blurred margins within the choroid (Fig. 1). Choroidal vascular hyperpermeability was evaluated in the late phase of IA by an experienced ophthalmologist (SO) who was masked to the EDI-OCT images. In the present study, all eyes with choroidal vascular hyperpermeability showed minimal extension of the focal hyperfluorescent area.

OCT System and Thickness Measurement

Choroidal thickness was measured using the EDI technique,[15] which was performed by placing the SD-OCT (Spectralis; Heidelberg Engineering) instrument close enough to the eye to obtain an inverted image. All images were obtained using an eye-tracking system, and 100 scans were averaged automatically to improve the signal-to-noise ratio. The subfoveal choroidal thickness, defined as the vertical distance between the hyperreflective line of Bruch's membrane and the chorioscleral interface, was measured using the horizontal and vertical line scans through the center of the fovea. All measurements were performed manually using a built-in caliber by a trained ophthalmologist (PJ) blinded to the study parameters including diagnosis, angiographic findings, and genotype. Each thickness was determined as the mean thickness using vertical and horizontal B-scan images through the center of the fovea.

In B-scans where it was difficult to identify the entire outer choroid, 5–10 points at which the chorioscleral interface could be identified were chosen and connected to create a segmentation line. The subfoveal choroidal thickness was measured after the segmentation lines were created. If the thickness differed remarkably between the horizontal and vertical B-scans, the segmentation lines of the B-scans were rechecked and corrected as required.

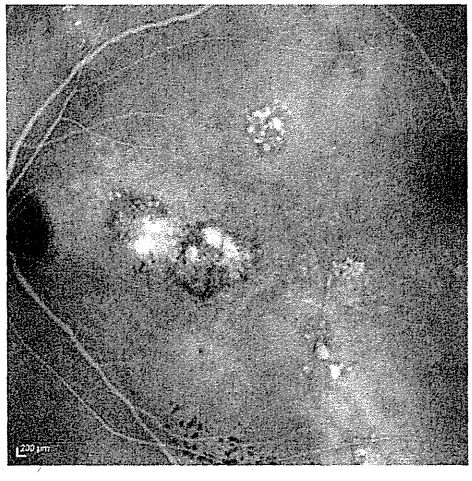

FIGURE 1. Choroidal vascular hyperpermeability. Choroidal vascular hyperpermeability was evaluated in the late phase of indocyanine green angiography (IA), 10–15 minutes after injection of dye. Choroidal hyperpermeability is seen as multifocal areas of hyperfluorescence with blurred margins.

Treatments

Patients who had a visual disturbance due to typical AMD and PCV were offered anti-VEGF therapy or PDT combined with anti-VEGF therapy. All eyes treated by intravitreous ranibizumab monotherapy ($n = 63$; 31 eyes with typical AMD and 32 eyes with PCV) received three successive intravitreal injections of ranibizumab at monthly intervals. Injections of ranibizumab were performed under sterile conditions, and prophylactic topical antibiotics were applied for 1 week after the injection.

In all eyes treated by PDT combined with intravitreal ranibizumab ($n = 16$; 10 eyes with typical AMD and 6 eyes with PCV), ranibizumab injections were performed in a sterile manner and prophylactic topical antibiotics were applied for 1 week after the injection. At 3–4 days after the intravitreal injection of ranibizumab, normal-fluence PDT was performed using a 689-nm diode laser unit (Visulas PDT system 690S; Carl Zeiss Meditec, Dublin, CA) after an injection of verteporfin, according to PDT guidelines for AMD. The greatest linear dimension chosen was based on fluorescein and indocyanine green angiograms. All polypoidal lesions, the entire vascular network, and choroidal neovascularization (CNV) detected with fluorescein or indocyanine green angiography were included.

Genotyping

Genomic DNA was prepared from peripheral blood leukocytes of 86 patients (41 patients with typical AMD and 45 patients with PCV) with a DNA extraction kit (QuickGene-610L; Fujifilm, Tokyo, Japan). We genotyped the major AMD-associated SNPs, *CFH* Y402 rs1061170, *CFH* I62V rs800292, and *ARMS2* A69S rs10490924, using SNP genotyping assays (*Taq*Man SNP Assay, ABI PRISM 7700 system; Applied Biosystems, Inc., Foster City, CA) according to the manufacturer's instructions. To evaluate the association of choroidal thickness or choroidal hyperpermeability and genotyping, data from the right eye were selected in patients with bilateral diseases.

Statistical Analyses

An independent sample *t*-test was used to compare variables between typical AMD eyes and PCV eyes, and between eyes with unilateral disease and unaffected fellow eyes. The paired-sample *t*-test was used to compare mean choroidal thickness before and after treatment. To evaluate the genotype effect, an allelic χ^2 test 2×2 table was used. To evaluate choroidal thickness trends according to each genotype, the Jonckheere-Terpstra test was used. All statistical evaluations were performed using commercially available software (SPSS20; IBM, Armonk, NY). Values of $P < 0.05$ were considered to indicate statistical significance.

TABLE 1. Demographic Data and Subfoveal Choroidal Thickness in Typical AMD and PCV

	Typical AMD	PCV	P Value (t-test)
n	64	65	
Age (y)	76.3 6 8.1	73.3 6 8.0	0.037
Refractive error (diopter)	0.6 6 2.0	0.1 6 1.8	0.152
Subfoveal CT (μm)	203.6 6 105.9	243.3 6 92.9	0.025

CT, choroidal thickness.

RESULTS

In the present study, 64 eyes of 58 patients and 65 eyes of 63 patients were diagnosed as typical AMD and PCV, respectively. Mean age was 76.3 6 8.1 years in patients with AMD and 73.3 6 8.0 years in patients with PCV ($P = 0.037$, *t*-test). The mean refractive error was 0.6 6 2.0 diopters in eyes with typical AMD and 0.1 6 1.8 diopters in eyes with PCV ($P = 0.152$, *t*-test) (Table 1).

Choroidal Thickness in Typical AMD and PCV

The mean subfoveal choroidal thickness was significantly thinner in eyes with typical AMD (203.6 6 105.9 μm) than that in eyes with PCV (243.4 6 92.9 μm, $P = 0.025$, *t*-test) (Table 1). In patients older than 70 years of age, subfoveal choroidal thickness was significantly thinner in eyes with typical AMD (169.6 6 89.4 μm) than that in eyes with PCV (236.3 6 87.0 μm, $P < 0.001$, *t*-test). In typical AMD, the mean subfoveal choroidal thickness in eyes with choroidal vascular hyperpermeability on IA was significantly greater than that in eyes without it ($P < 0.001$, *t*-test) (Figs. 2 and 3, Table 2).

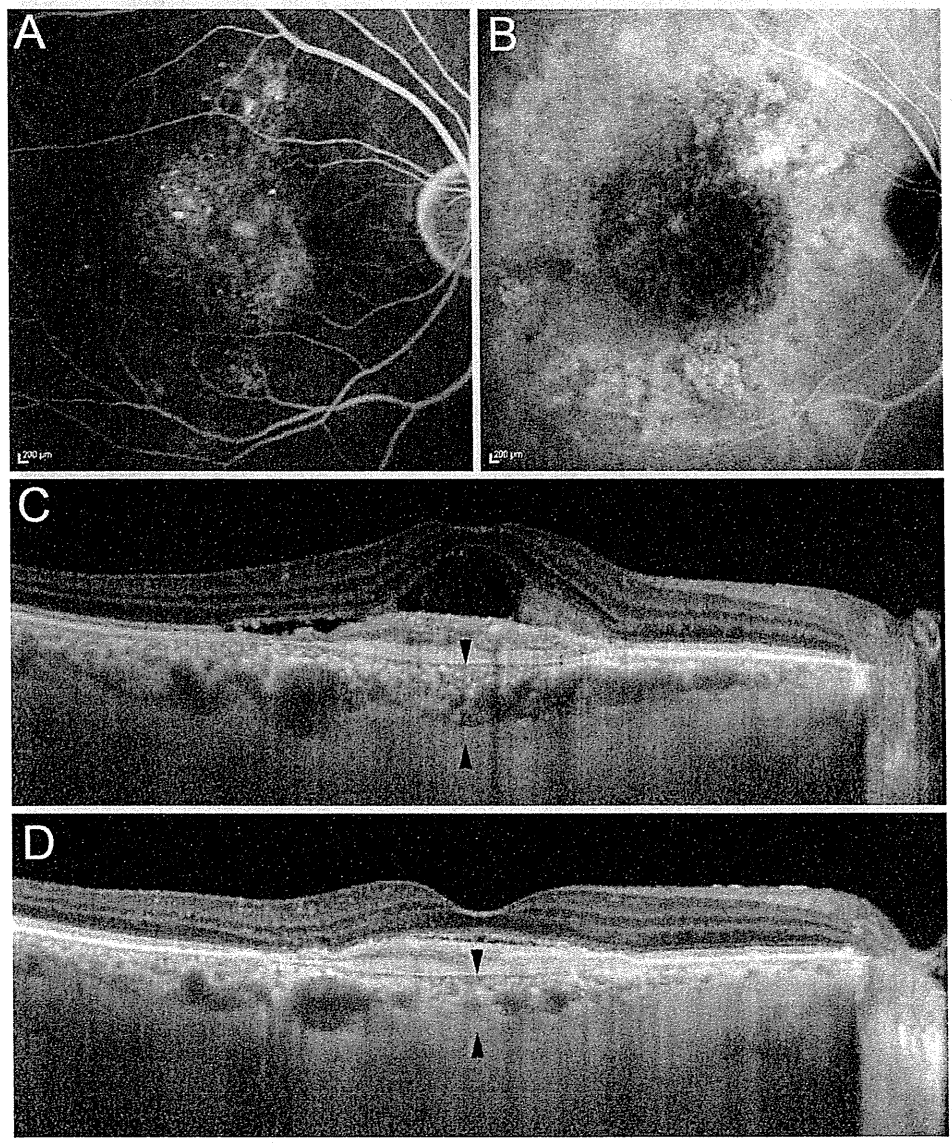

FIGURE 2. Typical AMD with choroidal hyperpermeability. (**A**) FA shows late leakage. (**B**) Late-phase IA shows choroidal vascular hyperpermeability. (**C**) EDI-OCT shows SRD, subretinal exudation, fibrovascular PED, and thick choroid. Subfoveal choroidal thickness was 320 μm (*between arrowheads*). (**D**) At 3 months after photodynamic therapy combined with intravitreal ranibizumab, EDI-OCT shows almost resolved SRD and decreased choroidal thickness. Subfoveal choroidal thickness was 258 μm (*between arrowheads*).

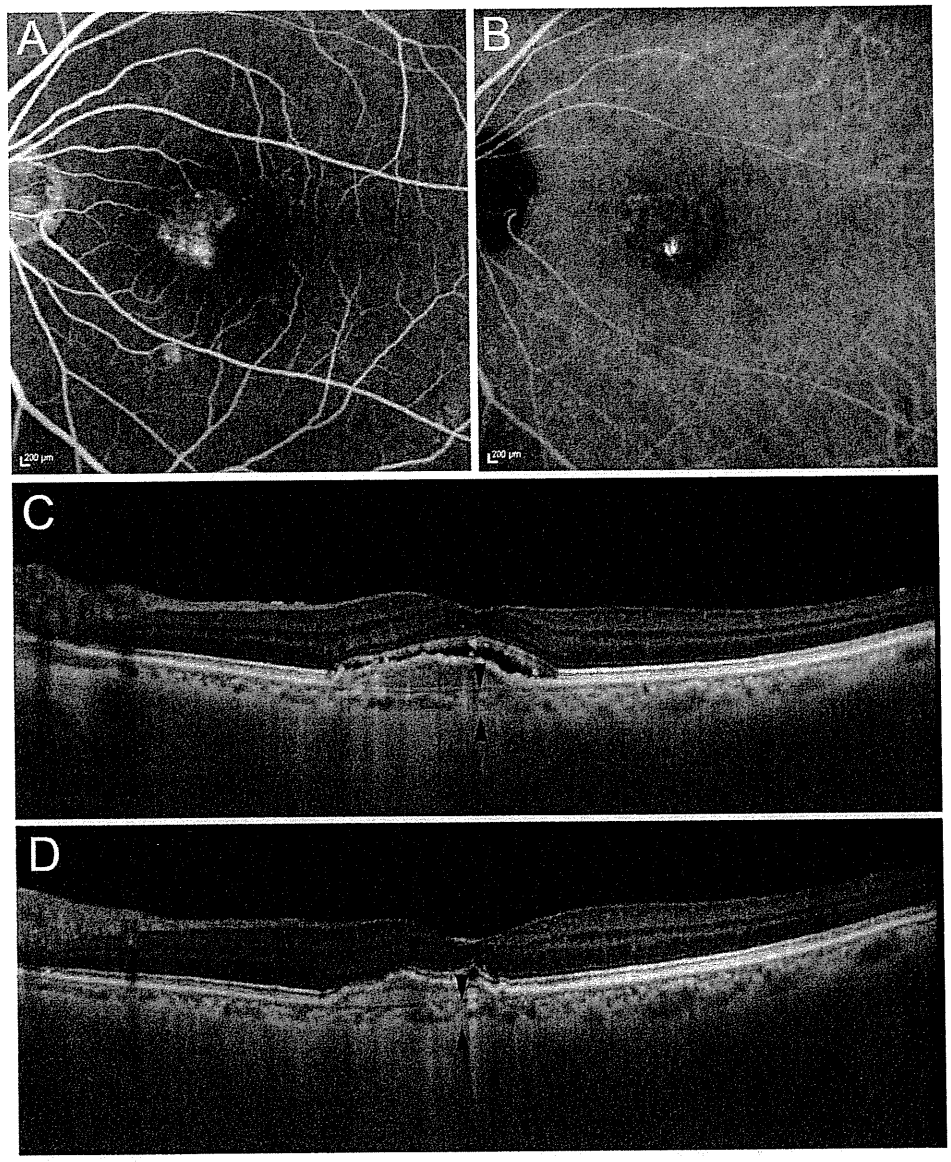

FIGURE 3. Typical AMD without choroidal hyperpermeability. (A) FA shows late leakage. (B) Late-phase IA shows no choroidal hyperpermeability. (C) EDI-OCT shows SRD, fibrovascular PED, and thin choroid. Subfoveal choroidal thickness was 134 μm (*between arrowheads*). (D) After 3 monthly injections of intravitreal ranibizumab, EDI-OCT shows resolution of SRD and stable choroidal thickness. Subfoveal choroidal thickness was 134 μm (*between arrowheads*).

Similarly in PCV, the mean subfoveal choroidal thickness in eyes with choroidal vascular hyperpermeability on IA was significantly greater than that in eyes without it ($P = 0.020$, *t*-test) (Figs. 4 and 5, Table 2).

In eyes with choroidal hyperpermeability, mean subfoveal choroidal thickness was similar between eyes with typical AMD and PCV ($P = 0.848$, *t*-test) (Table 2). In contrast, in eyes without choroidal vascular hyperpermeability, the mean

TABLE 2. Subfoveal Choroidal Thickness and Choroidal Hyperpermeability

		With Choroidal Hyperpermeability	Without Choroidal Hyperpermeability	P Value (t-test)
Typical AMD ($n = 64$)	*n*	24	40	
	Subfoveal CT (μm)	278.2 6 98.7 (μm)	158.9 6 83.1 (μm)	<0.001
PCV ($n = 65$)	*n*	20	45	
	Subfoveal CT (μm)	283.4 6 77.4 (μm)	225.7 6 94.5 (μm)	0.020
P value (*t*-test)		0.848	0.001	

CT, choroidal thickness.

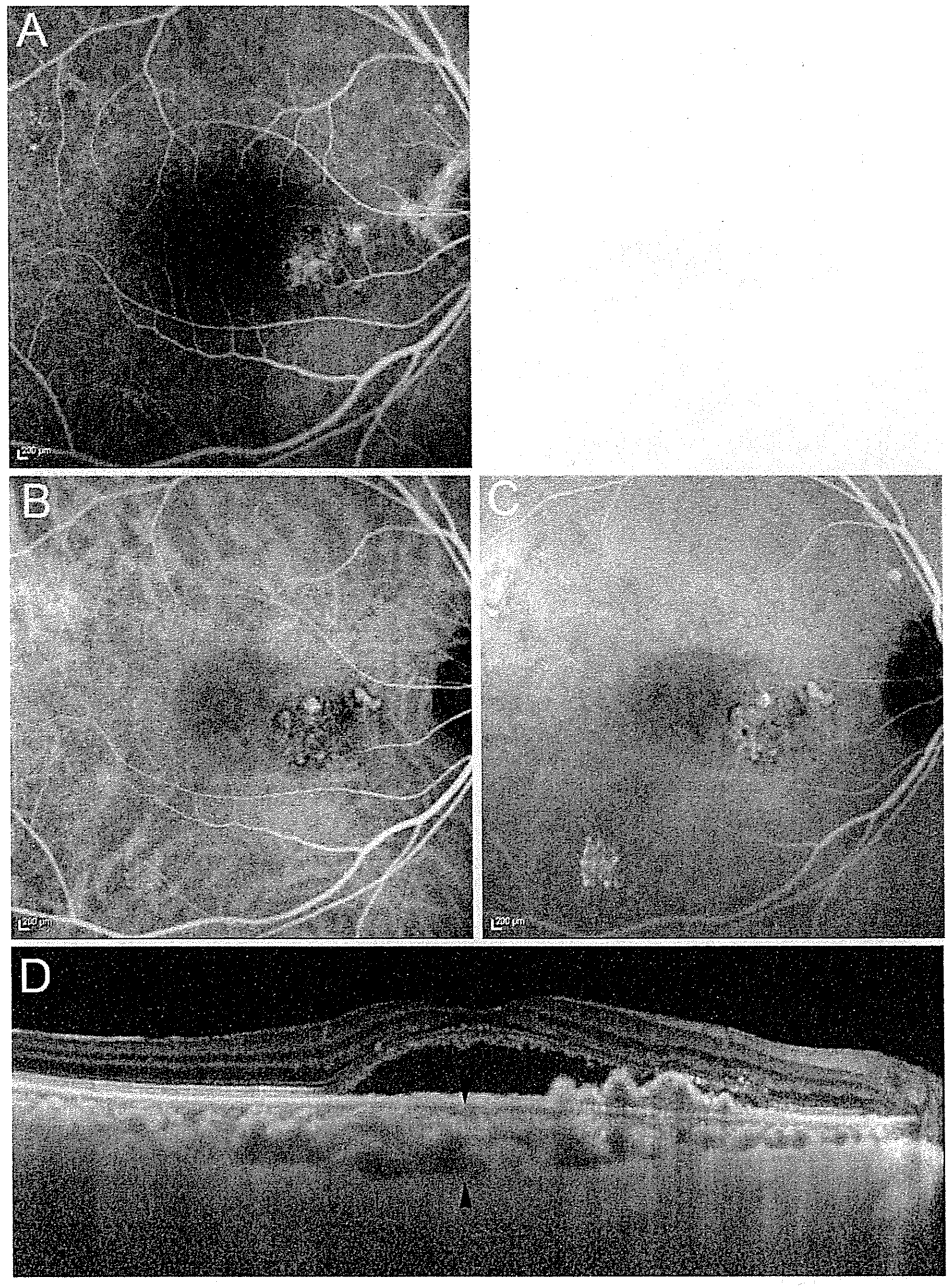

FIGURE 4. PCV with choroidal hyperpermeability. (**A**) FA shows late leakage. (**B**) Middle-phase IA shows a branching vascular network that terminates in polypoid lesions. (**C**) Late-phase IA shows choroidal vascular hyperpermeability. (**D**) EDI-OCT shows SRD, protrusions of the RPE suggesting polypoidal lesions, and thick choroid. Subfoveal choroidal thickness was 310 μm (*between arrowheads*).

subfoveal choroidal thickness was significantly greater in eyes with PCV than that in eyes with typical AMD ($P = 0.001$, *t*-test) (Figs. 3 and 5, Table 2).

Choroidal Thickness in Unilateral Disease Eyes and Fellow Eyes

In the present study, EDI-OCT had been performed in both eyes in 101 patients with unilateral diseases; thus, subfoveal choroidal thickness in unilateral disease eyes and fellow eyes was compared in these patients. In patients with unilateral typical AMD and PCV, no significant difference was observed between the mean subfoveal choroidal thickness in disease eyes and fellow eyes ($P = 0.938$ in typical AMD and $P = 0.996$ in PCV, *t*-test) (Table 3). Mean subfoveal choroidal thickness was significantly thinner in eyes with typical AMD than that in eyes with PCV both in disease eyes ($P = 0.023$, *t*-test) and in fellow eyes ($P = 0.026$, *t*-test) (Table 3). In the fellow eyes of patients with typical AMD, the mean subfoveal choroidal thickness was significantly greater in eyes with choroidal vascular hyperpermeability on IA than that in eyes without it ($P < 0.001$, *t*-test) (Table 4). Similarly, in the fellow eyes of patients with PCV, the mean subfoveal choroidal thickness was significantly greater in eyes with choroidal vascular hyperpermeability on IA than that in eyes without it ($P = 0.027$, *t*-test) (Table 4).

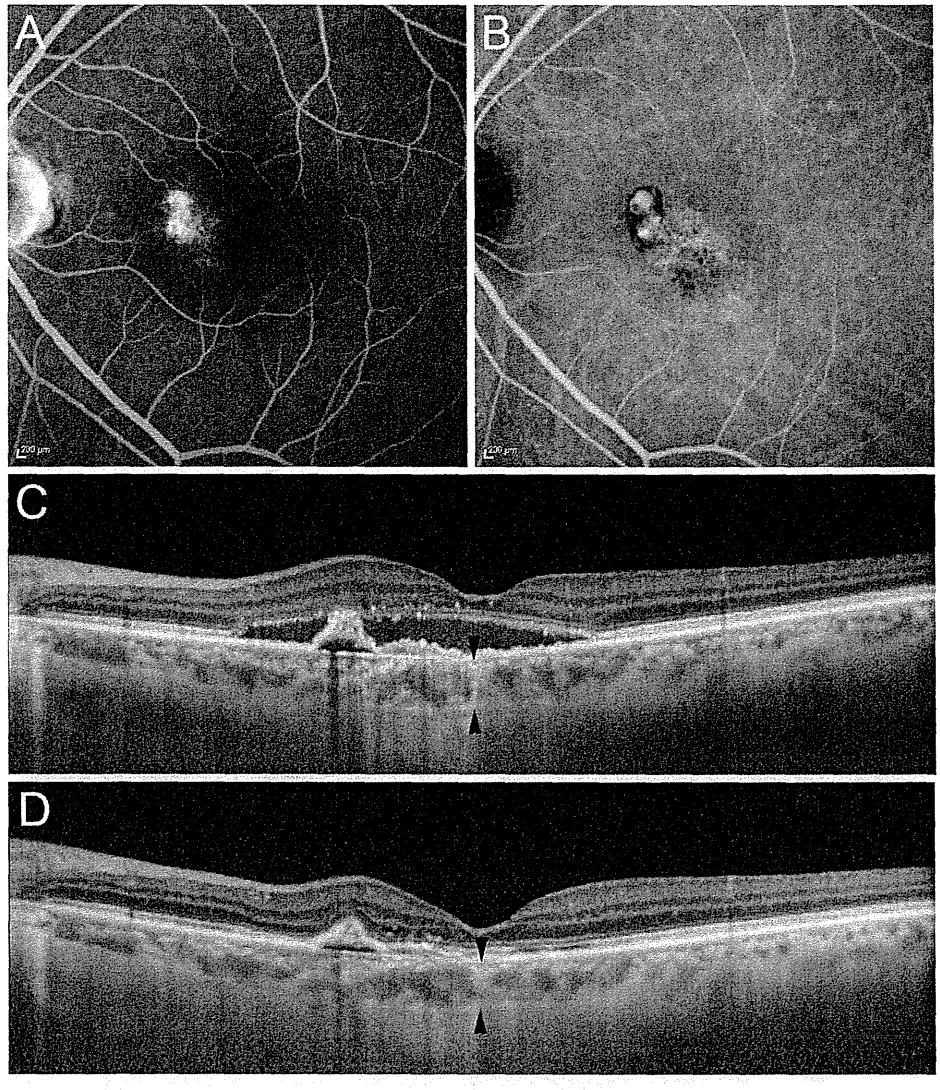

FIGURE 5. PCV without choroidal hyperpermeability. (A) FA shows late leakage. (B) Late-phase IA shows a branching vascular network that terminates in polypoid lesions, but shows no choroidal hyperpermeability. (C) EDI-OCT shows SRD, protrusions of the RPE, and thinner choroid compared with Figure 4. Subfoveal choroidal thickness was 230 μm (*between arrowheads*). (D) After 3 monthly injections of intravitreal ranibizumab, EDI-OCT shows resolution of SRD and almost stable choroidal thickness. Subfoveal choroidal thickness was 222 μm (*between arrowheads*).

In eyes with choroidal hyperpermeability, mean subfoveal choroidal thickness was not different between the fellow eyes of patients with typical AMD and PCV ($P = 0.401$, *t*-test) (Table 4). In contrast, in eyes without choroidal vascular hyperpermeability, the mean subfoveal choroidal thickness was significantly greater in the fellow eyes of patients with PCV than that in the fellow eyes of patients with typical AMD ($P = 0.004$, *t*-test) (Table 4).

TABLE 3. Subfoveal Choroidal Thickness in Unilateral Disease Eyes and Fellow Eyes

	Disease Eyes	Fellow Eyes	P Value (t-test)
Typical AMD ($n = 47$)	202.1 6 88.4 (μm)	203.5 6 83.6 (μm)	0.938
PCV ($n = 54$)	242.3 6 86.6 (μm)	242.4 6 88.5 (μm)	0.996
P value (*t*-test)	0.023	0.026	

With bilateral choroidal hyperpermeability, mean subfoveal choroidal thickness was similar in eyes with typical AMD/PCV and fellow eyes (Table 5).

Choroidal Thickness Changes after Treatment

After combination therapy (PDT and intravitreous ranibizumab), the mean subfoveal choroidal thickness was decreased in typical AMD and PCV ($P = 0.054$ in eyes with choroidal hyperpermeability and $P = 0.010$ in eyes without choroidal hyperpermeability, paired *t*-test) (Table 6). In eyes with typical AMD, subfoveal choroidal thickness decreased from 234.7 6 114.2 to 191.4 6 111.2 μm 3 months after PDT combined with intravitreal ranibizumab ($P = 0.016$, paired *t*-test) (Fig. 2). In eyes with PCV, subfoveal choroidal thickness decreased from 201.0 6 101.1 to 172.9 6 91.0 μm 3 months after PDT combined with intravitreal ranibizumab ($P = 0.036$, paired *t*-test). In contrast, three injections of intravitreous ranibizumab did not decrease subfoveal choroidal thickness in typical AMD

TABLE 4. Subfoveal Choroidal Thickness and Choroidal Hyperpermeability in Fellow Eyes

		With Choroidal Hyperpermeability	Without Choroidal Hyperpermeability	P Value (t-test)
Fellow eyes of typical AMD (n = 47)	n	19	28	
	Subfoveal CT (μm)	258.6 6 69.8 (μm)	166.1 6 71.1 (μm)	<0.001
Fellow eyes of PCV (n = 54)	n	17	37	
	Subfoveal CT (μm)	280.4 6 83.8 (μm)	224.8 6 83.5 (μm)	0.027
P value (t-test)		0.401	0.004	

CT, choroidal thickness.

and PCV ($P = 0.415$ in eyes with choroidal hyperpermeability and $P = 0.173$ in eyes without choroidal hyperpermeability, paired t-test) (Table 6, Figs. 3 and 5).

Visual acuity improved after monthly injections of intravitreal ranibizumab regardless of choroidal hyperpermeability (Table 7). In contrast, visual acuity was stable after PDT combined with intravitreal ranibizumab regardless of choroidal hyperpermeability (Table 7).

Genomic Association

The I62V polymorphism in the *CFH* gene seemed to contribute to choroidal thickness. Mean subfoveal choroidal thickness was 247.5 6 97.7 μm in genotype AA, 248.2 6 97.6 μm in genotype GA, and 221.9 6 102.7 μm in genotype GG (P = 0.117, Jonckheere-Terpstra test) (Fig. 6). Specifically in eyes with PCV, mean subfoveal choroidal thickness was 274.9 6 79.0 μm in genotype AA, 273.9 6 99.2 μm in genotype GA, and 219.5 6 90.0 μm in genotype GG ($P = 0.043$, Jonckheere-Terpstra test) (Fig. 6). In contrast, the Y402H polymorphism in the *CFH* gene and the A69S polymorphism in the *ARMS2* gene did not contribute to subfoveal choroidal thickness ($P = 0.461$ and 0.248, respectively, Jonckheere-Terpstra test).

The frequency of the minor allele in *CFH* I62V polymorphism was 34% in patients with choroidal hyperpermeability and 24% in patients without choroidal hyperpermeability (Table 8). Upon analyzing the genotypes using the 2 × 2 table from the allelic χ^2 test, the G allele did not contribute to choroidal hyperpermeability (P = 0.169). The T allele and C allele in *CFH* Y402H and *ARMS2* A69S, respectively, also did not contribute to choroidal hyperpermeability ($P = 0.575$ and 0.244, respectively).

DISCUSSION

Several researchers have reported on the subfoveal choroidal thickness in eyes with PCV and typical AMD.[21-24] However, little is known about the relationship between choroidal thickness and angiographic changes or genotypes in these eyes. In the present study, we investigated a consecutive series of treatment-naïve patients with typical AMD and PCV and found a relationship between choroidal thickness and subtypes of AMD, choroidal vascular hyperpermeability, and polymorphisms in the *CFH* gene in these diseases.

TABLE 5. Subfoveal Choroidal Thickness in Disease Eyes and Fellow Eyes with Bilateral Choroidal Hyperpermeability

	Disease Eyes	Fellow Eyes	P Value (t-test)
Typical AMD (n = 7)	251.6 6 87.9	258.3 6 80.7	0.885
PCV (n = 11)	274.8 6 96.2	255.2 6 77.5	0.606
P value (t-test)	0.615	0.937	

Subfoveal choroidal thickness was reported to be greater in eyes with PCV than that in eyes with typical AMD,[22-24] which is consistent with the present study. In addition, in the present study, subfoveal choroidal thickness of the fellow eyes was greater in eyes with PCV than that in eyes with typical AMD. These differences in choroidal thickness may indicate a significant structural difference in the choroid between typical AMD and PCV.

In eyes without choroidal vascular hyperpermeability, the mean subfoveal choroidal thickness was significantly greater in eyes with PCV than that in eyes with typical AMD. The same was true in the fellow eyes of patients with typical AMD and PCV. Thus, in eyes without choroidal hyperpermeability, the difference in choroidal thickness may reflect the different pathologic mechanisms of the two diseases. The decreased ability of the choroid to deliver oxygen and other metabolites to the retina, which is due mainly to choroidal blood volume rather than velocity of flow, has been postulated to lead to CNV in typical AMD.[27] Our results showing thinner choroidal thickness in eyes with typical AMD may be explained by this postulation. In addition, dilation of choroidal vessels and a collection of dilated thin-walled vessels derived from choroidal vessels beneath the retinal pigment epithelium (RPE) have been noted in histopathologic studies of PCV.[28-31] The present results regarding choroidal thickness of PCV may reflect those of histologic studies.

Choroidal thickness has a relationship not only with subtypes of AMD but also with choroidal vascular hyperpermeability. Maruko et al.[21] reported that choroid in PCV eyes with choroidal hyperpermeability was thicker than that in eyes without choroidal hyperpermeability, consistent with the present study. We first showed that, in typical AMD, the mean subfoveal choroidal thickness in eyes with choroidal vascular hyperpermeability on IA was significantly greater than that in eyes without it. In addition, in the fellow eyes of patients with typical AMD and PCV, the mean subfoveal choroidal thickness in eyes with choroidal vascular hyperpermeability on IA was significantly greater than that in eyes without it. These findings suggest that choroidal thickening is closely associated with choroidal hyperpermeability both in typical AMD and PCV, and both in disease eyes and fellow eyes. Thus, typical AMD and PCV may share, at least in part, a common pathology with choroidal vascular abnormalities with regard to choroidal hyperpermeability. In fact, in eyes with choroidal hyperpermeability, the mean choroidal thickness was similar between eyes with typical AMD and PCV. Hydrostatic pressure within the choroid may increase in areas with choroidal vascular hyperpermeability, resulting in increased extravascular volume within the choroid and increased choroidal thickness in typical AMD and PCV with choroidal hyperpermeability.

Recently, Maruko et al.[21] reported that subfoveal choroidal thickness was decreased by PDT monotherapy and PDT combined with intravitreous ranibizumab in eyes with PCV. In the present study, after PDT combined with intravitreous

TABLE 6. Mean Subfoveal Choroidal Thickness Change before and after Treatment in Eyes with and without Choroidal Vascular Hyperpermeability

	Treatment (n)	Baseline	3-Month Follow-up	P Value (t-test)
With choroidal hyperpermeability	PDT + IVR (6)	292.8 6 89.2	240.1 6 103.4	0.054
	Mono-IVR (20)	286.1 6 105.5	288.1 6 106.2	0.415
Without choroidal hyperpermeability	PDT + IVR (10)	170.3 6 97.4	133.1 6 82.4	0.010
	Mono-IVR (43)	200.8 6 106.4	198.0 6 109.0	0.173

Treatment consisted of intravitreal ranibizumab monotherapy or PDT combined with intravitreal ranibizumab. IVR, intravitreal ranibizumab.

TABLE 7. Mean logMAR BCVA before and after treatment in Eyes with and without Choroidal Vascular Hyperpermeability

	Treatment (n)	Baseline	3-Month Follow-up	P Value (t-test)
With choroidal hyperpermeability	PDT + IVR (6)	0.46 6 0.28	0.34 6 0.39	0.314
	Mono-IVR (20)	0.41 6 0.36	0.33 6 0.33	0.040
Without choroidal hyperpermeability	PDT + IVR (10)	0.76 6 0.55	0.64 6 0.59	0.226
	Mono-IVR (43)	0.49 6 0.43	0.42 6 0.41	0.014

Treatment consisted of intravitreal ranibizumab monotherapy or PDT combined with intravitreal ranibizumab. IVR, intravitreal ranibizumab.

ranibizumab, the mean subfoveal choroidal thickness was decreased in both typical AMD and PCV. Taken together, PDT leads to choroidal thinning not only in PCV but also in typical AMD eyes, whereas intravitreal ranibizumab has less effect on choroidal thickness in these diseases. These findings may be reflective of the different treatment effects of PDT on typical AMD and PCV.[3,7] Choroidal thickness is lower in typical AMD than that in PCV; thus, additional thinning of the choroid after PDT may have adverse effects and influence visual prognosis, especially in typical AMD.

Existing evidence suggests an association between AMD and polymorphisms in the *CFH* and *ARMS2* genes.[32–35] In a Japanese cohort, we have shown that three single nucleotide polymorphisms of *CFH* Y402H, I62V, and *ARMS2* A69S are associated with typical AMD and PCV.[36] However, possible associations between choroidal thickness and genetic background remained unknown. In the present study, the I62V polymorphism in the *CFH* gene seemed to contribute to choroidal thickness in patients with PCV. *CFH* expression has been shown to occur primarily in the RPE, drusen, and choroidal capillaries.[32] *CFH* is a critical negative regulator of

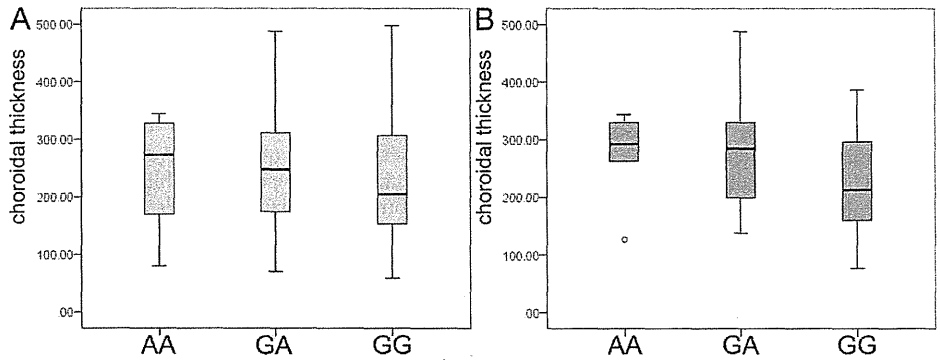

FIGURE 6. Subfoveal choroidal thickness and I62V polymorphism in the complement factor H gene. (**A**) Eyes with typical AMD and PCV. Mean choroidal thickness was 247.5 6 97.7 μm in genotype AA, 248.2 6 97.6 μm in genotype GA, and 221.9 6 102.7 μm in genotype GG. (**B**) Eyes with PCV. Mean choroidal thickness was 274.9 6 79.0 μm in genotype AA, 273.9 6 99.2 μm in genotype GA, and 219.5 6 90.0 μm in genotype GG.

TABLE 8. Distribution of *ARMS2* A69S, *CFH* I62V, and *CFH* Y402 Genotypes in Patients with and without Choroidal Hyperpermeability

	Hyperpermeability (+)					Hyperpermeability (-)					
	Genotype, No. (%)			Allele, No. (%)		Genotype, No. (%)			Allele, No. (%)		P *
ARMS2 A69S	GG	GT	TT	G	T	GG	GT	TT	G	T	
	6 (19)	15 (47)	11 (34)	27 (42)	37 (58)	7 (13)	22 (41)	25 (46)	36 (33)	72 (67)	0.244
CFH I62V	AA	GA	GG	A	G	AA	GA	GG	A	G	
	5 (16)	11 (35)	15 (48)	21 (34)	41 (66)	4 (7)	18 (33)	32 (59)	26 (24)	82 (76)	0.169
CFH Y402	CC	CT	TT	C	T	CC	CT	TT	C	T	
	1 (3)	5 (16)	26 (81)	7 (11)	57 (89)	1 (2)	13 (24)	40 (74)	15 (14)	93 (86)	0.575

*P value from allelic χ^2 test 2 × 2 table for its exact counterpart. *ARMS2*, age-related maculopathy susceptibility 2; *CFH*, complement factor H.

the alternative pathway of the complement system.[32] The association between *CFH* and choroidal thickness in PCV leads to the hypothesis that inflammation may be involved in the choroidal thickness changes in PCV. A histopathologic study demonstrated infiltration of T and B lymphocytes present throughout the choroid in an eye with PCV and infiltration of macrophages among PCV lesions,[37] suggesting that inflammation is implicated in the pathogenesis of PCV. Further genetic study in a large cohort should deepen our understanding of the clinical significance of choroidal thickness and choroidal hyperpermeability, which may be involved in the pathology of typical AMD and PCV.

This study has some limitations. In addition to the retrospective nature of the study and lack of controls, the choroidal thickness in all images was evaluated manually because no automated computer software is available to calculate choroidal thickness. Although EDI-OCT increases the sensitivity of the choroid, light scattering by the RPE and choroid still occurs; this hampers visualization of the choriosclera interface in some patients, especially in eyes with a very thick choroid. In such eyes, 5–10 points at which the choriosclera interface could be identified were chosen and connected to form a segmentation line, and the subfoveal choroidal thickness was measured. Despite these limitations, we found that choroidal thickness was associated with subtypes of AMD, choroidal hyperpermeability, and polymorphisms in the *CFH* gene. Choroidal thickness was greater in PCV than that in typical AMD. Choroidal thickness was greater in eyes with choroidal hyperpermeability, both in typical AMD and PCV, and both in disease eyes and fellow eyes. In eyes without choroidal hyperpermeability, EDI-OCT is useful as an auxiliary measure for differentiating typical AMD and PCV. PDT combined with intravitreal ranibizumab decreased the choroidal thickness both in typical AMD and PCV; thus, a lengthy follow-up study is needed for evaluating this combined therapy. Further research on the association of inflammation and choroidal structure will deepen our understanding of the pathology of these diseases.

References

1. Maruko I, Iida T, Saito M, Nagayama D, Saito K. Clinical characteristics of exudative age-related macular degeneration in Japanese patients. *Am J Ophthalmol.* 2007;144:15–22.
2. Yannuzzi LA, Sorenson J, Spaide RF, Lipson B. Idiopathic polypoidal choroidal vasculopathy (IPCV). *Retina.* 1990;10:1–8.
3. Otani A, Sasahara M, Yodoi Y, et al. Indocyanine green angiography: guided photodynamic therapy for polypoidal choroidal vasculopathy. *Am J Ophthalmol.* 2007;114:7–14.
4. Brown DM, Michels M, Kaiser PK, Heier JS, Sy JP, Ianchulev T; ANCHOR Study Group. Ranibizumab versus verteporfin photodynamic therapy for neovascular age-related macular degeneration: two-year results of the ANCHOR study. *Ophthalmology.* 2009;116:57–65.
5. Saito M, Iida T, Nagayama D. Photodynamic therapy with verteporfin for age-related macular degeneration or polypoidal choroidal vasculopathy: comparison of the presence of serous retinal pigment epithelial detachment. *Br J Ophthalmol.* 2008;92:1642–1647.
6. Gomi F, Sawa M, Sakaguchi H, et al. Efficacy of intravitreal bevacizumab for polypoidal choroidal vasculopathy. *Br J Ophthalmol.* 2008;92:70–73.
7. Kokame GT, Yeung L, Lai JC. Continuous anti-VEGF treatment with ranibizumab for polypoidal choroidal vasculopathy: 6-month results. *Br J Ophthalmol.* 2010;94:297–301.
8. Guyer DR, Yannuzzi LA, Slankter JS, et al. Digital indocyanine green angiography of central serous chorioretinopathy. *Arch Ophthalmol.* 1994;112:1057–1062.
9. Piccolino FC, Borgia L. Central serous chorioretinopathy and indocyanine green angiography. *Retina.* 1994;14:231–242.
10. Spaide RF, Hall L, Haas A, et al. Indocyanine green video-angiography of older patients with central serous chorioretinopathy. *Retina.* 1996;16:203–213.
11. Iida T, Kishi S, Hagimura N, et al. Persistence and bilateral choroidal vascular abnormality in central serous chorioretinopathy. *Retina.* 1999;19:508–512.
12. McLeopod DS, Taomoto M, Otsuji T, et al. Quantifying changes in RPE and choroidal vasculature in eyes with age-related macular degeneration. *Invest Ophthalmol Vis Sci.* 2002;43:1986–1993.
13. Sasahara M, Tsujikawa A, Musashi K, et al. Polypoidal choroidal vasculopathy with choroidal vascular hyperpermeability. *Am J Ophthalmol.* 2006;142:601–607.
14. Tsujikawa A, Ojima Y, Yamashiro K, et al. Punctate hyperfluorescent spots associated with central serous chorioretinopathy as seen on indocyanine green angiography. *Retina.* 2010;30:801–809.
15. Spaide RF, Koizumi H, Pozonni MC. Enhanced depth imaging spectral-domain optical coherence tomography. *Am J Ophthalmol.* 2008;146:496–500.
16. Margolis R, Spaide RF. Pilot study of enhanced depth imaging optical coherence of tomography of the choroid in normal eyes. *Am J Ophthalmol.* 2009;147:811–815.
17. Imamura Y, Fujiwara, T, Margolis R, Spaide RF. Enhanced depth imaging optical coherence tomography of the choroid in central serous chorioretinopathy. *Retina.* 2009;29:1469–1473.
18. Maruko I, Iida T, Sugano Y, et al. Subfoveal choroidal thickness after treatment of central serous chorioretinopathy. *Ophthalmology.* 2010;117:1792–1799.
19. Maruko I, Iida T, Sugano Y, et al. Subfoveal choroidal thickness in fellow eyes of patients with central serous chorioretinopathy. *Retina.* 2011;31:1603–1608.
20. Maruko I, Iida T, Sugano Y, Saito M, Sekiryu T. One-year choroidal thickness results after photodynamic therapy for central serous chorioretinopathy. *Retina.* 2011;21:1921–1927.
21. Maruko I, Iida T, Sugano Y, et al. Subfoveal retinal and choroidal thickness after verteporfin photodynamic therapy for polypoidal choroidal vasculopathy. *Am J Ophthalmol.* 2011;151:594–603.
22. Koizumi H, Yamagishi T, Yamazaki T, Kawasaki R, Kinoshita S. Subfoveal choroidal thickness in typical age-related macular degeneration and polypoidal choroidal vasculopathy. *Graefes Arch Clin Exp Ophthalmol.* 2011;249:1123–1128.
23. Chung SE, Kang SW, Lee JH, Kim YT. Choroidal thickness in polypoidal choroidal vasculopathy and exudative age-related macular degeneration. *Ophthalmology.* 2010;118:840–845.
24. Kim SW, Oh J, Kwon SS, Yoo J, Huh K. Comparison of choroidal thickness among patients with healthy eyes, early age-related macular degeneration, central serous chorioretinopathy and polypoidal vasculopathy. *Retina.* 2011;31:1904–1911.
25. Maruko I, Iida T, Sugano Y, et al. Subfoveal choroidal thickness after treatment of Vogt-Koyanagi-Harada disease. *Retina.* 2011;31:510–517.
26. Reibaldi M, Boscia F, Avitabile T, et al. Enhanced depth imaging optical coherence tomography of choroid in idiopathic macular hole: a cross-sectional prospective study. *Am J Ophthalmol.* 2011;151:112–117.
27. Grossniklaus HE, Green WR. Choroidal neovascularization. *Am J Ophthalmol.* 2004;137:496–503.
28. Lafaut BA, Aisenbrey S, Van den Broecke C, Bartz-Schmidt KU, Heimann K. Polypoidal choroidal vasculopathy pattern in age-

related macular degeneration: a clinicopathologic correlation. *Retina*. 2000;20:650–654.

29. Rosa RH Jr, Davis JL, Eifrig CW. Clinicopathologic reports, case reports, and small case series: clinicopathologic correlation of idiopathic polypoidal choroidal vasculopathy. *Arch Ophthalmol*. 2002;120:502–508.
30. Terasaki H, Miyake Y, Suzuki T, Nakamura M, Nagasaka T. Polypoidal choroidal vasculopathy treated with macular translocation: clinical pathological correlation. *Br J Ophthalmol*. 2002;86:321–327.
31. Okubo A, Sameshima M, Uemura A, Kanda S, Ohba N. Clinicopathological correlation of polypoidal choroidal vasculopathy revealed by ultrastructural study. *Br J Ophthalmol*. 2002;86:1093–1098.
32. Klein RJ, Zeiss C, Chew EY, et al. Complement factor H polymorphism in age-related macular degeneration. *Science*. 2005;308:385–389.
33. Haines JL, Hauser MA, Schmidt S, et al. Complement factor H variant increases the risk of age-related macular degeneration. *Science*. 2005;308:419–421.
34. Edwards AO, Ritter R 3rd, Abel KJ, Manning A, Panhuysen C, Farrer LA. Complement factor H polymorphism and age-related macular degeneration. *Science*. 2005;308:421–424.
35. Schmidt S, Hauser MA, Scott WK, et al. Cigarette smoking strongly modifies the association of LOC387715 and age-related macular degeneration. *Am J Hum Genet*. 2006;78:852–864.
36. Hayashi H, Yamashiro K, Gotoh N, et al. CFH and ARMS2 variations in age-related macular degeneration, polypoidal choroidal vasculopathy, and retinal angiomatous proliferation. *Invest Ophthalmol Vis Sci*. 2010;51:5914–5919.
37. MacCumber MW, Dastgheib K, Bressler NM, et al. Clinicopathologic correlation of the multiple recurrent serosanguineous retinal pigment epithelial detachments syndrome. *Retina*. 1994;14:143–152.

Association of Genetic Variants on 8p21 and 4q12 with Age-Related Macular Degeneration in Asian Populations

Isao Nakata,[1,2] Kenji Yamashiro,[1] Yumiko Akagi-Kurashige,[1,2] Masahiro Miyake,[1,2] Kyoko Kumagai,[1] Akitaka Tsujikawa,[1] Ke Liu,[3] Li Jia Chen,[3] David T. L. Liu,[3] Timothy Y. Y. Lai,[3] Yoichi Sakurada,[4] Seigo Yoneyama,[4] Ching-Yu Cheng,[6-9] Peter Cackett,[6] Ian Y. Yeo,[6] Wan Ting Tay,[6] Belinda K. Cornes,[6] Eranga N. Vithana,[6,7] Tin Aung,[6,7] Keitaro Matsuo,[10] Fumihiko Matsuda,[2] Tien-Yin Wong,[6,7,11] Hiroyuki Iijima,[4] Chi Pui Pang,[3] and Nagahisa Yoshimura[1]

Purpose. To evaluate the association of genetic variants at chromosomes 8p21 and 4q12 with the risk of developing AMD and its two main subtypes, choroidal neovascular membrane (CNV) and polypoidal choroidal vasculopathy (PCV), in Asian populations.

Methods. The study population comprised 2360 patients with neovascular AMD (1013 typical AMD-CNV and 1282 PCV), and 3598 controls from four independent cohorts, two of Japanese (n = 4859) and two of Chinese (n = 1099) ethnicity. We performed a meta-analysis in case-control studies of two reported single nucleotide polymorphisms (SNPs) (rs13278062 at *TNFRSF10A-LOC389641* on 8p21 and rs1713985 at *REST-C4orf14-POLR2B-IGFBP7* on 4q12) by using logistic regression analysis adjusted for age and sex. Subgroup analysis by CNV and PCV subtypes were performed to evaluate the significance of these two variants.

Results. The reported association between rs13278062 at 8p21 and neovascular AMD was replicated in this population ($P = 1.12 \times 10^{-4}$, odds ratio [OR] = 0.79, 95% confidence interval [CI] = 0.70–0.89). However, there was no association of rs1713985 at 4q12 with neovascular AMD, or its two subtypes, typical AMD-CNV and PCV (all $P > 0.05$). The study sample size had a statistical power of greater than 99% to detect an association of a risk allele with AMD with an OR of 1.30, as reported in the original study of rs1713985 and AMD.

Conclusions. The present results did not replicate the reported association between rs1713985 at 4q12 and neovascular AMD. However, we confirmed the association between rs13278062 at 8p21 and neovascular AMD in Asian populations. (*Invest Ophthalmol Vis Sci.* 2012;53:6576–6581) DOI:10.1167/iovs.12-10219

From the [1]Department of Ophthalmology and the [2]Center for Genomic Medicine/Inserm U.852, Kyoto University Graduate School of Medicine, Kyoto, Japan; the [3]Department of Ophthalmology and Visual Sciences, The Chinese University of Hong Kong, Hong Kong, China; the [4]Department of Ophthalmology, Faculty of Medicine, University of Yamanashi, Yamanashi, Japan; the [6]Singapore Eye Research Institute and Singapore National Eye Centre, Singapore; the [7]Department of Ophthalmology, Yong Loo Lin School of Medicine and the [8]Saw Swee Hock School of Public Health, National University of Singapore, Singapore; the [9]Centre for Quantitative Medicine, Office of Clinical Sciences, Duke-NUS Graduate Medical School, Singapore; the [10]Division of Epidemiology and Prevention, Aichi Cancer Center Research Institute, Nagoya, Japan; and the [11]Centre for Eye Research Australia, University of Melbourne, Australia.

Supported by grants in part by grants-in-aid for scientific research (19390442, 22791706, 23791972, and 22791653) from the Japan Society for the Promotion of Science, Tokyo, Japan; by the Japanese National Society for the Prevention of Blindness; by funding from the American Health Assistance Foundation (M2011068); by a Endowment Fund for Lim Por-Yen Eye Genetics Research Centre and the General Research Fund from the Research Grants Council (473410), Hong Kong; and by grants from the SingHealth, Singapore (SHF/FG381P/2007), the National Medical Research Council, Singapore (STaR/0003/2008), and the Biomedical Research Council, Singapore (BMRC 09/1/35/19/616 and 08/1/35/19/550).

Submitted for publication May 18, 2012; revised July 27, 2012; accepted August 24, 2012.

Disclosure: **I. Nakata**, None; **K. Yamashiro**, None; **Y. Akagi-Kurashige**, None; **M. Miyake**, None; **K. Kumagai**, None; **A. Tsujikawa**, None; **K. Liu**, None; **L.J. Chen**, None; **D.T.L. Liu**, None; **T.Y.Y. Lai**, None; **Y. Sakurada**, None; **S. Yoneyama**, None; **C.-Y. Cheng**, None; **P. Cackett**, None; **I.Y. Yeo**, None; **W.T. Tay**, None; **B.K. Cornes**, None; **E.N. Vithana**, None; **T. Aung**, None; **K. Matsuo**, None; **F. Matsuda**, None; **T.-Y. Wong**, None; **H. Iijima**, None; **C.P. Pang**, None; **N. Yoshimura**, None

Corresponding author: Kenji Yamashiro, Department of Ophthalmology and Visual Sciences, Kyoto University Graduate School of Medicine, 54 Kawahara, Shogoin, Sakyo, Kyoto 606-8507, Japan; yamashro@kuhp.kyoto-u.ac.jp.

AMD is the leading cause of visual impairment in the elderly and the most common cause of blindness in developed countries.[1] Several genes have been reported to be associated with this disease,[2-10] and these genetic studies have helped to reveal the mechanisms underlying the development of AMD, specifically suggesting an inflammation-based model of AMD pathogenesis.[11-13]

There is increasing recognition that the prevalence of AMD in Asian populations is as high as in Caucasian populations.[14] However, it has been suggested that the frequency of AMD subtypes may differ between the Asians and Caucasians.[15,16] In Asian populations, neovascular AMD ("wet" AMD) is the major type of late AMD, and is associated with choroidal neovascular membrane (CNV), collectively referred to as AMD-CNV in this study. However, recent studies revealed that almost all reported genetic risk factors for developing AMD in Asians are identical to those for developing Caucasian AMD.[17-20]

Polypoidal choroidal vasculopathy (PCV) is the other subtype of neovascular AMD, and it is usually diagnosed clinically by indocyanine green angiography.[21] The prevalence of PCV in Asian populations with neovascular AMD has been reported to be higher than in Caucasians.[22-24] Previous studies

Investigative Ophthalmology & Visual Science, September 2012, Vol. 53, No. 10
Copyright 2012 The Association for Research in Vision and Ophthalmology, Inc.